MIKE
Powered by DHI

MIKE 21 & MIKE 3 Flow Model

Advection-Dispersion Module

Scientific Documentation

DHI headquarters
Agern Allé 5
DK-2970 Hørsholm
Denmark

+45 4516 9200 Telephone
+45 4516 9333 Support
+45 4516 9292 Telefax

mike@dhigroup.com
www.mikepoweredbydhi.com

PLEASE NOTE

CONTENTS

MIKE 21 & MIKE 3 FLOW MODEL
Advection-Dispersion Module
Scientific Documentation

1 Introduction 1

2 Numerical Schemes 2
2.1 General Description 2
2.2 An Explicit Scheme for Advection-Dispersion Modelling in Two Dimensions 4
2.3 Advection-Dispersion Modelling in Three Dimensions 15

3 Dispersion Coefficients 29
3.1 General Description 29
3.2 Dispersive Processes 30
3.2.1 General 30
3.2.2 Turbulence 31
3.2.3 Shear flows 32
3.2.4 Subgrid scale processes 34
3.3 Estimation of Coefficients in 2D Modelling 35
3.3.1 Basic formulations 35
3.3.2 The evidence of experience 38
3.3.3 A general interpretation 40

4 Heat Dissipation 42

5 Flooding and Drying 43
5.1 General 43
5.2 Flooding due to External Sources 43
5.3 Flooding due to a High Water Level in Neighbour Cells 44
5.3.1 Chain flooding for the first time 44
5.3.2 Chain flooding on previously wet cell 45
5.4 Drying 45

6 List of Symbols 46

7 List of References 47

1 Introduction

The present Scientific Documentation aims to give a description of the equations and numerical formulation used in the Advection-Dispersion (AD) module of the MIKE 21 Flow Model and MIKE 3 Flow Model.

The equation for the Advection-Dispersion module is shown below. The numerical schemes for the calculations are described in Chapter 2. The numerical algorithm and solution technique applied in the model is described in the paper “An Explicit Scheme for Advection-Dispersion Modelling in Two Dimensions” in Section 2.2 and in the paper “Advection-Dispersion Modelling in Three Dimensions” in Section 2.3. This is followed by a discussion of Dispersion Coefficients, Chapter 3. The background for the Heat Dissipation formula is described briefly in Chapter 4, and finally, the background for the Flooding and Drying is described in Chapter 5.

The Advection-Dispersion module solves the so-called advection-dispersion equation for dissolved or suspended substances. This is in fact the mass-conservation equation. Discharge quantities and compound concentrations at source and sink points are included together with a decay rate.

$$\frac{\partial}{\partial t}(hc)+\frac{\partial}{\partial x}(uhc)+\frac{\partial}{\partial y}(vhc)+\frac{\partial}{\partial z}(whc)=\frac{\partial}{\partial x}\left(h\cdot D_x\cdot\frac{\partial c}{\partial x}\right)$$

$$+\frac{\partial}{\partial y}\left(h\cdot D_y\frac{\partial c}{\partial y}\right)++\frac{\partial}{\partial z}\left(h\cdot D_z\frac{\partial c}{\partial z}\right)-F\cdot h\cdot c+S \qquad (1.1)$$

Symbol list

c	compound concentration (arbitrary units)
u,v	horizontal velocity components in the x,y directions (m/s)
w	vertical velocity component in the z direction (m/s)
h	water depth (m)
D_x,D_y,D_z	dispersion coefficients in the x,y,z directions (m^2/s)
F	linear decay coefficient (sec^{-1})
S	$Q_s,(c_s-c)$
Q_s	source/sink discharge ($m^3/s/m^2$)
c_s	concentration of compound in the source/sink discharge.

Information on *u, v, w* and *h* at each time step is provided by the Hydrodynamic module.

2 Numerical Schemes

2.1 General Description

The transport of the scalar quantities, salinity and temperature is handled by a general advection-dispersion module. The general advection-dispersion equation reads,

$$\frac{\partial c}{\partial t} + \frac{\partial u_i c}{\partial x_i} = \frac{\partial}{\partial x_i}\left(D_i \frac{\partial c}{\partial x_i} \right) + SS \tag{2.1}$$

in which c is the scalar concentration variable, D_i the dispersion coefficients and SS a source-sink term.

MIKE 21 utilises an explicit scheme (QUICKEST) for the advection-dispersion modelling. The numerical algorithm and solution technique applied in the model is described in the paper “An Explicit Scheme for Advection-Dispersion Modelling in Two Dimensions” in Section 2.2

MIKE 3 offers four different advection-dispersion schemes:

- The fully 3D QUICKEST-SHARP scheme which is especially suitable for simulations with steep gradients
- The ULTIMATE-QUICKEST scheme with operator splitting and intermediate surface elevations calculated on basis of locally 1D continuity equations. The ULTIMATE-QUICKEST scheme is an alternative to the QUICKEST-SHARP scheme and it is designed to reduce computation time when more than one component has been selected
- The simple UPWIND scheme which is similar to the ULTIMATE-QUICKEST scheme except that upwinding is applied all over
- The fully 3D UPWIND scheme which is similar to the QUICKEST-SHARP scheme except that upwinding is applied all over

The numerical algorithm and solution technique for the 3D QUICKEST scheme is described in the paper “Advection-Dispersion Modelling in Three Dimensions” in Section 2.3. The information of u_i at each time step is provided by the hydrodynamic module and thus assumed constant throughout the time integration of the advection-dispersion equation. Unless otherwise specified the advection-dispersion equation is solved at each time step following the time integration of the hydrodynamic equations.

The ULTIMATE-QUICKEST and the simple UPWIND schemes have a built-in internal loop over components, which reduces the computation time when more components have been selected. With the QUICKEST-SHARP and the 3D UPWIND schemes the user may choose to turn on the “internal component loop”; this will increase the computational speed in cases with more than one component at the expense of requiring more memory during computations.

The schemes 3D QUICKEST-SHARP and the 3D UPWIND are so-called CWC schemes (for Consistency With Continuity), both designed to be consistent with the continuity equation (the mass equation) of the HD module. The CWC property is, however, not

always completely fulfilled with the non-hydrostatic HD engine due to the inherent compressibility of the ACM scheme.
For further details about the CWC schemes in MIKE 21 and MIKE 3, please see the separate Scientific Documentation MIKE 21 & MIKE 3 Flow Model, CWC Schemes – file name m3m21_cwc.pdf.

2.2 An Explicit Scheme for Advection-Dispersion Modelling in Two Dimensions

Computer Methods in Applied Mechanics and Engineering 88 (1991) 287–297
North-Holland

An explicit scheme for advection–diffusion modelling in two dimensions

Lars Ekebjærg[1] and Peter Justesen[1]
Institute of Hydrodynamics and Hydraulic Engineering (ISVA), Technical University of Denmark, DK-2800 Lyngby, Denmark

Received 6 November 1989
Revised manuscript received 8 June 1990

In this paper, an extension of the finite difference scheme QUICKEST for the advection–diffusion equation from one dimension into two dimensions is given. Advection as well as diffusion are formulated as transports leading to a very efficient scheme which lends itself to vectorization on supercomputers. The practicability of the scheme is tested using the lid-driven cavity flow as a test case and very good results are obtained.

1. Introduction

In recent years the third order finite difference scheme QUICKEST has appeared in various papers dealing with turbulence modelling, environmental modelling and similar areas, where the governing equation is the advection–diffusion equation. This is because the scheme in many ways has very fine qualities. It avoids the wiggle instability problem associated with central differencing of the advection terms, and at the same time it eliminates the numerical damping often experienced with first order upwinding methods (see [1]).

The scheme itself is a Lax–Wendroff or Leith-like scheme in the sense that it cancels out any truncation error terms due to time differencing up to a certain order by using the basic equation itself. In the case of QUICKEST, truncation error terms up to third order are cancelled, that is for both space and time derivatives. Readers interested in a more in-depth account of the schemes are referred to [2, 3].

The QUICKEST scheme was originally developed in [2] only for the one-dimensional case although giving some hints for the extension to higher dimensions. In papers where this scheme has been used in higher dimensions, it is evident that the extension to e.g. two dimensions by no means is as straight-forward as could be expected. None of the existing references come out with a clear two-dimensional counterpart of the original scheme. Some drop the diffusion part out of the equation (e.g. [4]) and others the cross-derivative terms [5]. Therefore the purpose of this note is to give a complete development of the 2D version of the QUICKEST scheme.

[1] Present address: Computational Hydraulics Centre (CHC), Danish Hydraulic Institute (DHI), DK-2970 Hørsholm.

2. The scheme

Consider the two-dimensional advection–diffusion equation

$$\frac{\partial c}{\partial t} + u\frac{\partial c}{\partial x} + v\frac{\partial c}{\partial y} = K_x\frac{\partial^2 c}{\partial x^2} + K_y\frac{\partial^2 c}{\partial y^2}\,, \tag{1}$$

where c is any scalar quantity transported by the steady velocity field (u, v) and diffused by the constant diffusion coefficients K_x and K_y. The mesh on which the equivalent finite difference equation is to be solved is depicted in Fig. 1.

From a Taylor series expansion of (1) around the point (j, k) the following equivalent finite difference equation is obtained:

$$\frac{c_{j,k}^{n+1} - c_{j,k}^{n}}{\Delta t} + u_{j,k}^{n}\frac{c_{j+1,k}^{n} - c_{j-1,k}^{n}}{2\Delta x} + v_{j,k}^{n}\frac{c_{j,k+1}^{n} - c_{j,k-1}^{n}}{2\Delta y}$$
$$= K_x\frac{c_{j+1,k}^{n} - 2c_{j,k}^{n} + c_{j-1,k}^{n}}{\Delta x^2} + K_y\frac{c_{j,k+1}^{n} - 2c_{j,k}^{n} + c_{j,k-1}^{n}}{\Delta y^2} + \mathrm{TE}\,, \tag{2}$$

where

$$\mathrm{TE} = \frac{\Delta t}{2}\frac{\partial^2 c}{\partial t^2} + \frac{\Delta t^2}{6}\frac{\partial^3 c}{\partial t^3} + u\frac{\Delta x^2}{6}\frac{\partial^3 c}{\partial x^3} + v\frac{\Delta y^2}{6}\frac{\partial^3 c}{\partial y^3} + \mathrm{HOT}\,, \tag{3}$$

HOT contains all fourth-order and higher truncation error terms, which in this development are to be neglected.

The next step in the development is to eliminate the time derivatives in (3). This can be done by differentiating (1) with respect to time:

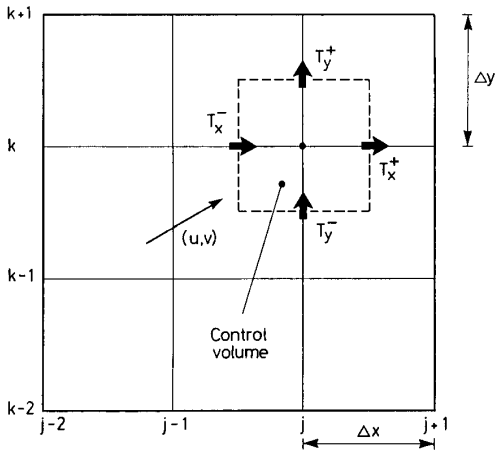

Fig. 1. Definition sketch.

$$\frac{\partial^2 c}{\partial t^2} = u^2 \frac{\partial^2 c}{\partial x^2} + 2uv \frac{\partial^2 c}{\partial x\,\partial y} + v^2 \frac{\partial^2 c}{\partial y^2}$$
$$- 2uK_x \frac{\partial^3 c}{\partial x^3} - 2vK_x \frac{\partial^3 c}{\partial x^2\,\partial y} - 2uK_y \frac{\partial^3 c}{\partial x\,\partial y^2} - 2vK_y \frac{\partial^3 c}{\partial y^3} \tag{4}$$

and

$$\frac{\partial^3 c}{\partial t^3} = -u^3 \frac{\partial^3 c}{\partial x^3} - 3u^2 v \frac{\partial^3 c}{\partial x^2\,\partial y} - 3uv^2 \frac{\partial^3 c}{\partial x\,\partial y^2} - v^3 \frac{\partial^3 c}{\partial y^3}\,. \tag{5}$$

If a flow direction as indicated in Fig. 1 is assumed, the following upwinded expression can be given for the third order derivatives:

$$\frac{\partial^3 c}{\partial x^3} = \frac{(c_{j+1,k} - 2c_{j,k} + c_{j-1,k}) - (c_{j,k} - 2c_{j-1,k} + c_{j-2,k})}{\Delta x^3}\,, \tag{6}$$

$$\frac{\partial^3 c}{\partial x^2\,\partial y} = \frac{(c_{j+1,k} - 2c_{j,k} + c_{j-1,k}) - (c_{j+1,k-1} - 2c_{j,k-1} + c_{j-1,k-1})}{\Delta x^2\,\Delta y}\,, \tag{7}$$

and likewise for $\partial^3 c/\partial y^3$ and $\partial^3 c/\partial x\,\partial y^2$.

The last term to be put on difference form is $\partial^2 c/\partial x\,\partial y$. This is done through

$$\frac{\partial^2 c}{\partial x\,\partial y} = \frac{c_{j,k} - c_{j-1,k} - c_{j,k-1} + c_{j-1,k-1}}{\Delta x\,\Delta y} + \mathrm{TE}'\,. \tag{8}$$

As can be seen, (8) is also upwinded. This upwinding implies that the indices have to be adjusted according to the local flow direction.

The truncation error term in (8) is given by

$$\mathrm{TE}' = \frac{\Delta x}{2} \frac{\partial^3 c}{\partial x^2\,\partial y} + \frac{\Delta y}{2} \frac{\partial^3 c}{\partial x\,\partial y^2} \tag{9}$$

and is modelled according to (7).

Finally, substituting (3)–(9) into (2) and defining the Courant numbers and dimensionless diffusivities

$$C_x = u\frac{\Delta t}{\Delta x}\,, \qquad \Gamma_x = K_x \frac{\Delta t}{\Delta x^2}\,, \qquad C_y = v\frac{\Delta t}{\Delta y}\,, \qquad \Gamma_y = K_y \frac{\Delta t}{\Delta y^2}\,,$$

we obtain after some rearrangement

$$\begin{aligned} c_{j,k}^{n+1} = c_{j,k}^n \{ & 1 - 2(\tfrac{1}{2}C_x^2 + \Gamma_x) + C_x C_y - 2(\tfrac{1}{2}C_y^2 + \Gamma_y) - 3(\tfrac{1}{6}C_x - \tfrac{1}{6}C_x^3 - C_x\Gamma_x) \\ & - 3(\tfrac{1}{6}C_y - \tfrac{1}{6}C_y^3 - C_y\Gamma_y) - 2(\tfrac{1}{2}C_x C_y - \tfrac{1}{2}C_x^2 C_y - C_y\Gamma_x) \\ & - 2(\tfrac{1}{2}C_x C_y - \tfrac{1}{2}C_x C_y^2 - C_x\Gamma_y)\} \\ + c_{j+1,k}^n \{ & -\tfrac{1}{2}C_x + (\tfrac{1}{2}C_x^2 + \Gamma_x) + (\tfrac{1}{6}C_x - \tfrac{1}{6}C_x^3 - C_x\Gamma_x) \\ & + (\tfrac{1}{2}C_x C_y - \tfrac{1}{2}C_x^2 C_y - C_y\Gamma_x)\} \end{aligned}$$

$$
\begin{aligned}
&+ c^n_{j,k+1}\{-\tfrac{1}{2}C_y + (\tfrac{1}{2}C_y^2 + \Gamma_y) + (\tfrac{1}{6}C_y - \tfrac{1}{6}C_y^3 - C_y\Gamma_y) \\
&\qquad + (\tfrac{1}{2}C_xC_y - \tfrac{1}{2}C_xC_y^2 - C_x\Gamma_y)\} \\
&+ c^n_{j-1,k}\{\tfrac{1}{2}C_x + (\tfrac{1}{2}C_x^2 + \Gamma_x) - C_xC_y + 3(\tfrac{1}{6}C_x - \tfrac{1}{6}C_x^3 - C_x\Gamma_x) \\
&\qquad + (\tfrac{1}{2}C_xC_y - \tfrac{1}{2}C_x^2C_y - C_y\Gamma_x) + 2(\tfrac{1}{2}C_xC_y - \tfrac{1}{2}C_xC_y^2 - C_x\Gamma_y)\} \\
&+ c^n_{j,k-1}\{\tfrac{1}{2}C_y - C_xC_y + (\tfrac{1}{2}C_y^2 + \Gamma_y) + 3(\tfrac{1}{6}C_y - \tfrac{1}{6}C_y^3 - C_y\Gamma_y) \\
&\qquad + 2(\tfrac{1}{2}C_xC_y - \tfrac{1}{2}C_x^2C_y - C_y\Gamma_x) + (\tfrac{1}{2}C_xC_y - \tfrac{1}{2}C_xC_y^2 - C_x\Gamma_y)\} \\
&+ c^n_{j-2,k}\{-(\tfrac{1}{6}C_x - \tfrac{1}{6}C_x^3 - C_x\Gamma_x)\} \\
&+ c^n_{j,k-2}\{-(\tfrac{1}{6}C_y - \tfrac{1}{6}C_y^3 - C_y\Gamma_y)\} \\
&+ c^n_{j-1,k-1}\{C_xC_y - (\tfrac{1}{2}C_xC_y - \tfrac{1}{2}C_x^2C_y - C_y\Gamma_x) \\
&\qquad - (\tfrac{1}{2}C_xC_y - \tfrac{1}{2}C_xC_y^2 - C_x\Gamma_y)\} \\
&+ c^n_{j-1,k+1}\{-(\tfrac{1}{2}C_xC_y - \tfrac{1}{2}C_xC_y^2 - C_x\Gamma_y)\} \\
&+ c^n_{j+1,k-1}\{-(\tfrac{1}{2}C_xC_y - \tfrac{1}{2}C_x^2C_y - C_y\Gamma_x)\} \,. \qquad (10)
\end{aligned}
$$

A computationally more convenient and efficient way of expressing the scheme, and more in accordance with the original development, is by the use of transports. Here the scheme can be written as

$$c^{n+1}_{j,k} = c^n_{j,k} + \{T_x^-(j,k) - T_x^+(j,k)\} + \{T_y^-(j,k) - T_y^+(j,k)\} \,, \qquad (11)$$

where the four transport terms are located as shown in Fig. 1. From the figure it is evident that

$$T_x^+(j-1,k) = T_x^-(j,k) \,, \qquad (12)$$

$$T_y^+(j,k-1) = T_y^-(j,k) \,; \qquad (13)$$

implying that (11) can be written as

$$c^{n+1}_{j,k} = c^n_{j,k} + \{T^n_x(j-1,k) - T^n_x(j,k)\} + \{T^n_y(j,k-1) - T^n_y(j,k)\} \,, \qquad (14)$$

where

$$T^n_x(j,k) = \alpha_1 c^n_{j+1,k} + \alpha_2 c^n_{j,k} + \alpha_3 c^n_{j-1,k} + \alpha_4 c^n_{j,k+1} + \alpha_5 c^n_{j,k-1} - \Gamma_x c^n_{j+1,k} + \Gamma_x c^n_{j,k} \qquad (15)$$

and

$$T^n_y(j,k) = \beta_1 c^n_{j,k+1} + \beta_2 c^n_{j,k} + \beta_3 c^n_{j,k-1} + \beta_4 c^n_{j+1,k} + \beta_5 c^n_{j-1,k} - \Gamma_y c^n_{j,k+1} + \Gamma_y c^n_{j,k} \,. \qquad (16)$$

Using (12)–(16) in connection with (10) leads to a series of isolated equations from which α_i and β_i can be determined. The α_i are given by

$$\alpha_1 = (\tfrac{1}{6}C_x^2 - \tfrac{1}{2}C_x + \tfrac{1}{3} + \Gamma_x)C_x \,, \tag{17a}$$

$$\alpha_2 = (-\tfrac{1}{3}C_x^2 + \tfrac{1}{2}C_x + \tfrac{5}{6} - \tfrac{1}{2}C_xC_y - \tfrac{1}{2}C_y^2 + \tfrac{1}{2}C_y - 2\Gamma_x - 2\Gamma_y)C_x \,, \tag{17b}$$

$$\alpha_3 = (-\tfrac{1}{6} + \tfrac{1}{6}C_x^2 + \Gamma_x)C_x \,, \qquad \alpha_4 = (-\tfrac{1}{2}C_y + \tfrac{1}{2}C_y^2 + \Gamma_y)C_x \,, \tag{17c, d}$$

$$\alpha_5 = (\tfrac{1}{2}C_xC_y + \Gamma_y)C_x \,. \tag{17e}$$

The corresponding expressions for β_i can be found by permutation of the x, y subscripts in (17). The positions of the weights for the determination of x- and y-transports are depicted in Fig. 2(a, b). When u and/or v are negative, the positions of α_i and β_i are changed accordingly such that the scheme is always upwinded. An example of the weight distribution for $(u<0, v>0)$ is given in Fig. 2(c, d) for the α_i and β_i, respectively. Note that the velocities which are used in the Courant numbers should be centered on the cell face across which the transport is to be determined.

It is important to notice that by using the concept of transports instead of the complete expression (10) for the scheme, the computational labour is significantly reduced. Furthermore, the explicit nature of the scheme means that it lends itself to vectorization on a supercomputer thus giving very fast execution times.

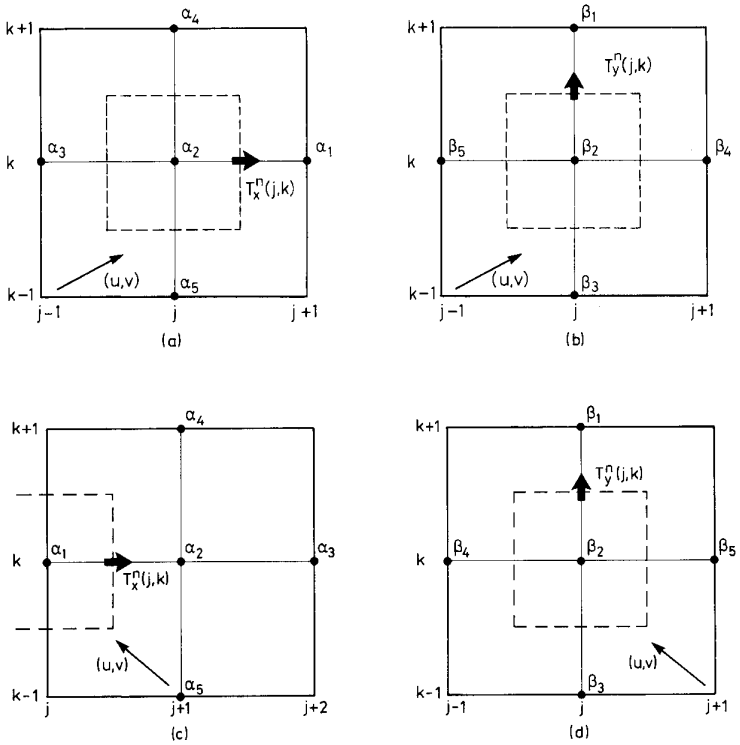

Fig. 2. Determination of x- and y-transports out of the cell (j, k). (a, b) $T_x^n(j, k)$ and $T_y^n(j, k)$ for $(u>0, v>0)$; (c, d) $T_x^n(j, k)$ and $T_y^n(j, k)$ *for* $(u<0, v>0)$.

Another advantage of this scheme is that solid boundaries are easy to handle because the transport vanishes across the boundary.

3. Stability analysis

For an explicit finite difference scheme it is very important to investigate the stability properties in order to assess its practical applicability. Thus a stability analysis in the Von Neumann sense of the scheme has been carried out. The results for the highest resolvable wave number from this analysis for various values of the Courant numbers and dimensionless diffusion coefficients are shown in Fig. 3.

As can be seen from the figure, in the diffusionless case the stability is bounded by the criterion of not letting the sum of the Courant numbers exceed unity. Further it is seen by comparing Fig. 3(a) and Fig. 3(b) that the introduction of diffusion increases the region of stability. The stable region will, however, diminish as the diffusion becomes dominant, cf. Fig. 3(c). In Fig. 3(d), the Courant numbers are fixed, and the dimensionless diffusivity is varied.

For a more detailed discussion of stability, the reader is referred to [2–4].

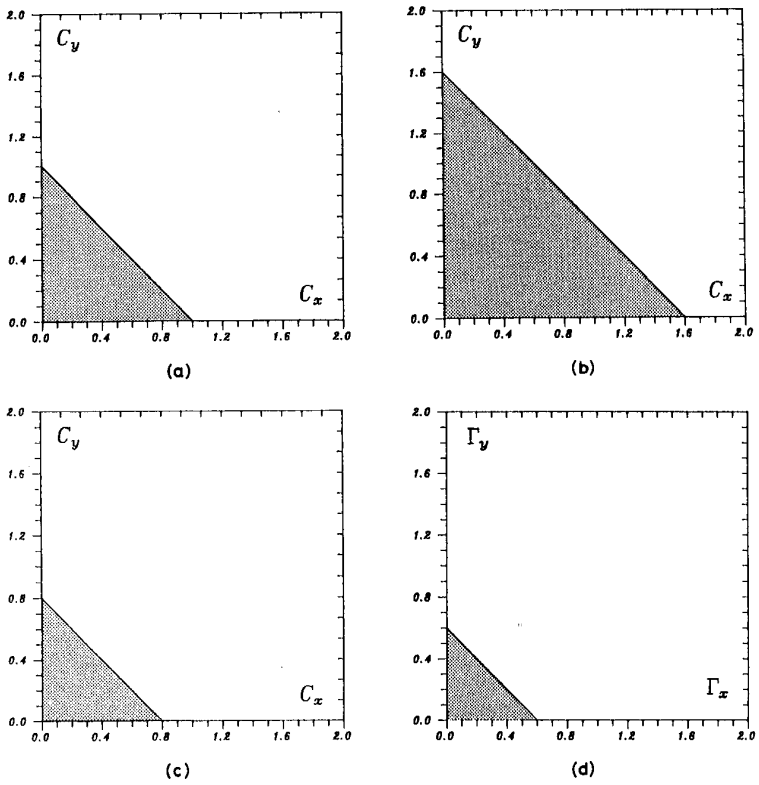

Fig. 3. Stability diagrams. Stable regions are shaded. (a) $\Gamma_x = \Gamma_y = 0$; (b) $\Gamma_x = \Gamma_y = 0.1$; (c) $\Gamma_x = \Gamma_y = 0.3$; (d) $C_x = C_y = 0.1$.

4. Test of the scheme

This section presents three test cases in order to illustrate the practicability of the scheme. The two first cases are the conventional tests with convected and rotated cones and the third case is a lid-driven cavity flow.

Convected cone

Five cases ($T1$–$T5$) of a cone which is convected in a uniform current field are presented. Table 1 gives the Courant numbers and dimensionless diffusivities in the tests and also the peak concentration and the change in total mass after a translation of 40 grid points relative to the initial values. Figure 4 depicts contours of concentrations after 0, 20 and 40 grid points of translation in four of the five tests.

From Table 1 it can be seen that the scheme possesses numerical diffusion giving a reduction in the peak concentration when the Courant number is not unity. Further, the scheme was unstable in $T4$ with Cr = 1.42 and $\Gamma_x = 0.0$. By adding diffusion ($\Gamma_x = 0.1$) in $T5$ a stable solution was obtained. This is in agreement with the stability analysis presented in Section 3. It can be noted that the scheme gives a very small mass falsification.

Rotated cone

Two cases ($R1$ and $R2$) of a cone which is convected in a rotating current field are presented. Table 2 gives the Courant numbers and dimensionless diffusivities in the tests and also the peak concentration and total mass at four instants during the first revolution relative to the initial values. Figure 5 depicts contours of concentrations after 0.25, 0.5, 0.75 and 1.0 revolution.

This test is more severe than the T-series since the transport now takes place at all angles to the grid since the velocity field is non-uniform. Again the scheme is seen to perform quite well.

Table 1
Convected cone tests. c_p is the peak concentration

Case	Cr	Γ_x	c_p	$\Delta \sum c_{j,k}$ (%)
$T1$	0.5	0.0	0.723	−0.15
$T2$	1.0	0.0	1.000	0.00
$T3$	1.0	0.1	0.255	−0.56
$T4$	1.42	0.0	unstable	N/A[a]
$T5$	1.42	0.1	0.308	−0.12

[a] N/A is 'not available'.

Table 2
Rotated cone tests. c_p is the peak concentration; n is the number of time steps. The Courant number is based on the velocity at the cone centre

Case	n	t/T	c_p	$\Delta \sum c_{j,k}$ (%)
$R1$	0	0.0	1.000	0.0
Cr = 0.25	64	0.25	0.728	−0.02
	128	0.5	0.634	−0.12
	192	0.75	0.570	−0.22
	256	1.00	0.524	−0.26
$R2$	0	0.0	1.000	0.0
Cr = 0.5	32	0.25	0.752	−0.02
	64	0.5	0.665	−0.13
	96	0.75	0.604	−0.23
	128	1.00	0.559	−0.27

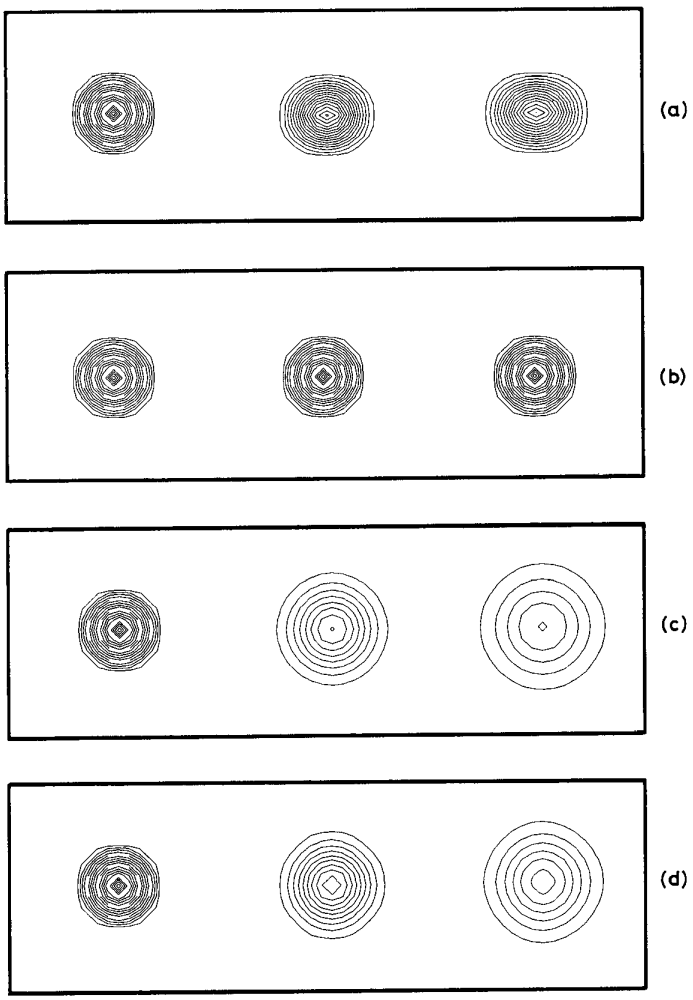

Fig. 4. Convected cone tests. The cones have been convected in a steady flow field according to Table 1. Initially the peak concentrations were 1.0 and contours of concentration are given after 0, 20 and 40 grid points of convection. $\Delta c = 0.05$. (a) $T1$; (b) $T2$, (c) $T3$; (d) $T5$.

Lid-driven cavity flow

In order to show the application of the scheme to a 'real' problem we have considered the lid-driven cavity flow which is a standard bench mark test case. A steady recirculating flow in a square cavity with length and height H is produced by moving the top lid at a constant speed U_L. The Navier–Stokes equations are written in two dimensions using the streamfunction vorticity formulation. No-slip conditions are imposed on the walls.

The present scheme has been used to integrate the vorticity transport equation whereas a standard successive overrelaxation (SOR) technique has been used to compute the new

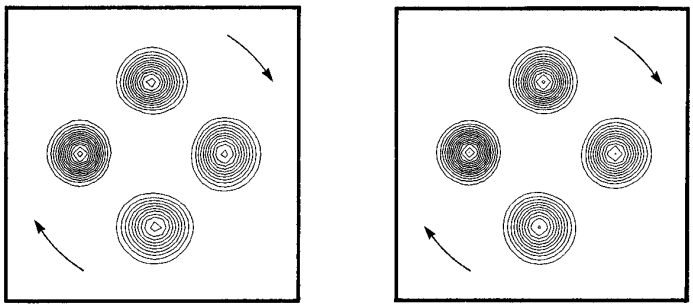

Fig. 5. Rotated cone tests. The cones have been convected in a rotating steady flow field according to Table 2. Initially the peak concentrations were 1.0 and contours of concentration are given after 0.25, 0.5, 0.75 and 1.0 revolutions. $\Delta c = 0.05$. (a) $R1$; (b) $R2$.

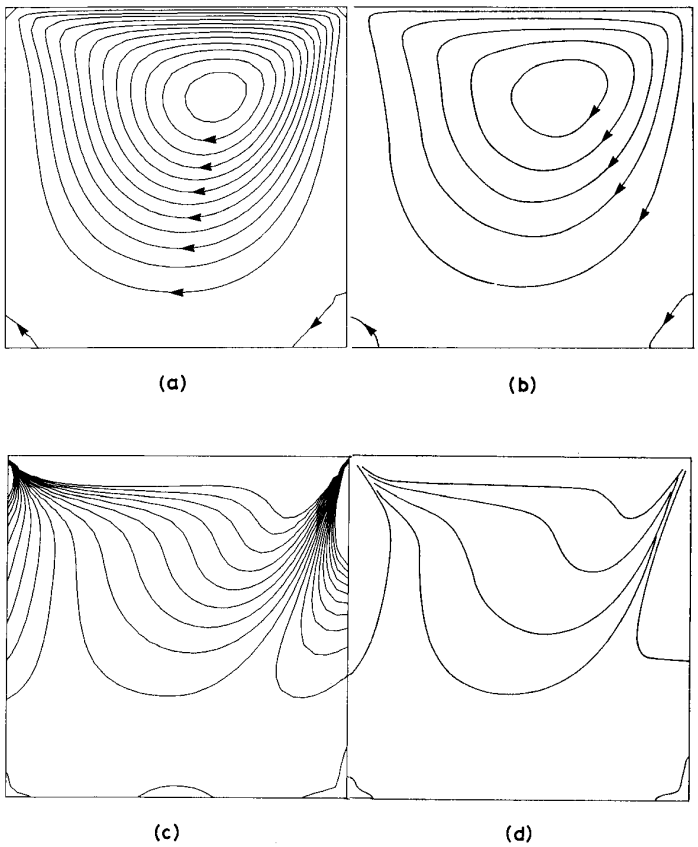

Fig. 6. Lid-driven cavity flow, Re = 100. (a) Streamfunction by present method (SOR); (b) Streamfunction in [6]; (c) Vorticity by present method (QUICKEST); (d) Vorticity in [6]. Note that contours are only indicative since they do not necessarily represent the same levels in the two sets of data.

streamfunction field at each time step. The steady solution has been found by integration in the time domain until the relative change in the solution was less than $\sim 10^{-5}$.

Figure 6 depicts the computed streamfunction and vorticity distributions in the steady solution for a Reynolds number Re = 100 where $\mathrm{Re} = U_L H/\nu$. 32 grid points were used in each direction and 2000 time steps were completed with $\Delta t = 0.007 H/U_L$ to reach the steady solution. The solution is compared with a similar solution obtained in [6] and an excellent agreement is observed. Also for Re = 400, the agreement is convincing, cf. Fig. 7. Again 32 grid points were used in each direction and 3000 time steps were completed with $\Delta t = 0.015 H/U_L$ to reach the steady solution.

When the Reynolds number is increased to 400 the solution changes such that the centre of the circulating eddy moves down towards the centre of the cavity. This can also be seen in Fig. 8 which depicts vertical profiles of the horizontal velocity in the centre of the cavity for both Reynolds numbers and by the present method as well as from [6]. The two sets of data agree very well and the Reynolds number effect is evident.

It is fully recognized that the present procedure does not necessarily represent the most efficient way of obtaining the steady solution for the lid-driven cavity flow. The test case serves as an example only.

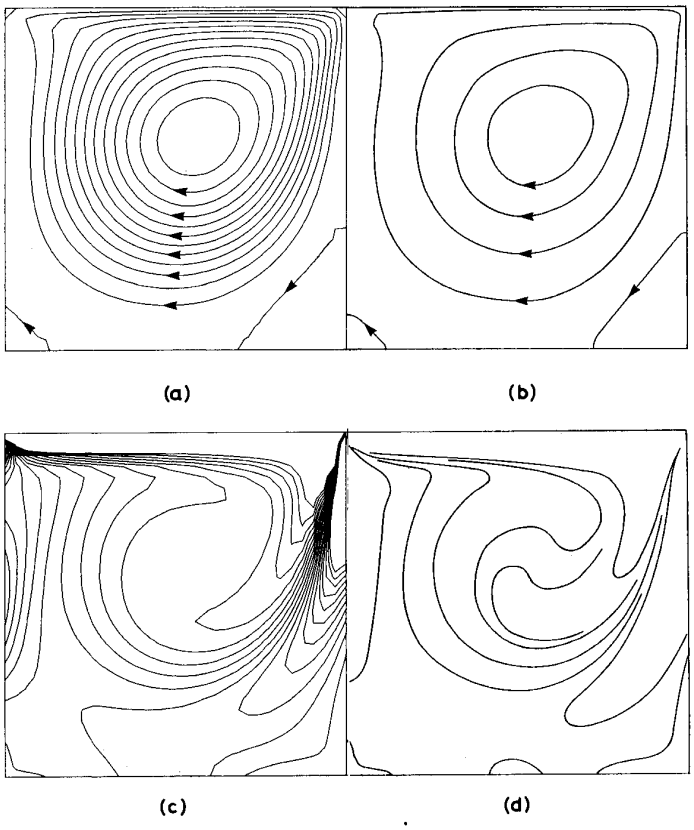

Fig. 7. Lid-driven cavity flow, Re = 400.

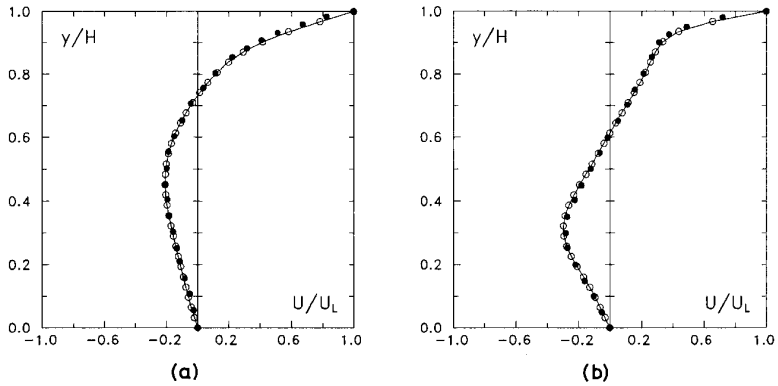

Fig. 8. Lid-driven cavity flow. Comparison of vertical profiles of the horizontal velocity in the centre of the cavity by the present method (——○——) and from [6] (●). (a) Re = 100; (b) Re = 400.

Acknowledgment

This work has been supported by the Danish Technical Research Council (STVF) through its FTU-programme 'Turbulens omkring offshorekonstruktioner'.

References

[1] S.V. Patankar, Numerical Heat Transfer and Fluid Flow (McGraw-Hill, New York, 1980).
[2] B.P. Leonard, A stable and accurate convective modelling procedure based on quadratic upstream interpolation, Comput. Methods Appl. Mech. Engrg. 19 (1979) 59–98.
[3] P.J. Roache, Computational Fluid Dynamics (Hermosa Publishers, Albuquerque, 1976).
[4] P. Justesen, K.W. Olesen and H.J. Vested, High-accuracy modelling of advection in two and three dimensions, in: Proc. IAHR 23rd Congress (Ottawa, Canada, 1989) D-239–D-246.
[5] R.W. Davis and E.F. Moore, A numerical study of vortex shedding from rectangles, J. Fluid Mech. 116 (1982) 475–506.
[6] O.R. Burggraf, Analytical and numerical studies of the structure of steady separated flows, J. Fluid Mech. 24 (1966) 113–151.

2.3 Advection-Dispersion Modelling in Three Dimensions

Advection-dispersion modelling in three dimensions

Hans Jacob Vested, Peter Justesen, and Lars Ekebjærg

Danish Hydraulic Institute, Hørsholm, Denmark

The explicit third-order-accurate finite-difference scheme QUICKEST for solving the advection-dispersion equation is extended to three dimensions. The scheme ensures mass conservation through the control volume formulation in transport terms. An analysis of the numerical stability is carried out, and stability diagrams are presented. Comparisons with three-dimensional analytical solutions as well as with other schemes are shown. The scheme is simple and computationally fast and thus is well suited for coupling to three-dimensional hydrodynamic models in order to simulate density-driven flows. An application from groundwater flow is also presented.

Keywords: advection-dispersion, QUICKEST, three dimensions, stability analysis

Introduction

Numerical modelling of advection-dispersion processes is an important aspect of many engineering problems. Advection-dispersion (AD) models are normally used to determine the spreading of neutrally buoyant substances, such as organic compounds or heavy metals, in the marine environment. The flow field is determined by a hydrodynamic (HD) model. The development of three-dimensional (3-D) numerical hydrodynamic models requires a coupling to AD models in order to calculate flows in which horizontal or vertical density gradients due to salinity or temperature variations exist.

The numerical solution of the AD equation using the finite difference methods is often invalidated by numerical dispersion, the presence of wiggles at fronts, and mass falsification.

A variety of numerical schemes have been developed with the purpose of overcoming these obstacles. Basically, these schemes can be divided into Eulerian and Lagrangian schemes, referring to whether a fixed or moving coordinate system is used in the computations. The Lagrangian schemes, taking advantage of the advection equation itself, can resolve fronts or discontinuities almost exactly (see, for example, Bode and Sobey[1]). The main problem in using Lagrangian schemes is the coupling of the transport description with the Eulerian hydrodynamic description upon which it depends, necessitating interfacing interpolation routines. Real turbulent flow will also complicate the Lagrangian mesh bookkeeping. However, for slowly varying flow fields (e.g., continental shelf circulation) the Lagrangian approach is an attractive method.[1] The Eulerian schemes on a fixed finite difference grid can produce wiggles or oscillations for higher-order schemes. Lower-order schemes (donor cell methods, upstream differencing) suffer from excessive numerical dispersion. Hybrid schemes have been developed that reduce these obstacles and are positive definite.[2]

An alternative numerical approach has been described by Leonard,[3] who introduced an upstream interpolation method in an explicit finite difference scheme for unsteady flow.

This scheme, named QUICKEST, was devised in one dimension to circumvent the problem of numerical dispersion of classical upwind differencing and the wiggles and stability problems introduced by central differencing. Another scheme, QUICK, was devised for quasi-steady flow. QUICKEST was used by Davis and Moore[4] to consider the flow around a cylinder in two dimensions. A survey of the state of the art in environmental transport modelling, published by the ASCE,[5] shows that only QUICK has been extensively used in three-dimensional transport modelling, whereas QUICKEST is not referenced. For a discussion of the QUICKEST scheme, see also Ref. 6.

QUICKEST is not in its formulation positive definite, as hybrid schemes are, but it provides an almost wiggle-free and accurate method for solving the AD equation. The explicit formulation ensures mass conservation through a control volume formulation, as well as being very simple to implement in a computer code. In a recent paper, Leonard[7] gives an extension of the QUICK scheme that eliminates the wiggles completely by introducing an exponential interpolation in regions with steep fronts.

Address reprint requests to Mr. Vested at the Danish Hydraulic Institute, Agern Allé 5, DK-2970 Hørsholm, Denmark.

Received 16 January 1991; revised 4 November 1991; accepted 2 April 1992

Flow problems involving AD processes are often unsteady and three-dimensional, making an extension of the QUICKEST scheme to three dimensions most relevant. A description of the use of QUICKEST in two and three dimensions is given by Justesen et al.[8] However, this version of the scheme did not include a compensation for the dispersion terms in the higher-order truncation error correction terms. Ekebjærg and Justesen[9] give a derivation of the QUICKEST scheme in two dimensions including these terms. The presence of a certain magnitude of dispersion improves the stability of the scheme in accordance with the original results of Leonard.[3]

In the following, a derivation of the QUICKEST scheme for three dimensions is given using the methodology of Ekebjærg and Justesen.[9] Although the derivation might appear to be rather complicated, the final formulation of the scheme as transport terms becomes very simple. The explicit scheme is, of course, limited by stability restrictions, and stability diagrams are presented. A series of analytical tests with the advection-dispersion of a 3-D Gaussian concentration distribution is described. The scheme is compared with a donor cell scheme[10] and the scheme of Smolarkiewicz.[11] Finally, an example of coupling with hydrodynamics and a practical application from groundwater modelling are shown.

Formulation of the scheme

The partial differential equation describing advection-dispersion can be written in conservation form as

$$\frac{\partial c}{\partial t} + \frac{\partial}{\partial x}(uc) + \frac{\partial}{\partial y}(vc) + \frac{\partial}{\partial z}(wc) = \frac{\partial}{\partial x}\left\{D_x \frac{\partial c}{\partial x}\right\} + \frac{\partial}{\partial y}\left\{D_y \frac{\partial c}{\partial y}\right\} + \frac{\partial}{\partial z}\left\{D_z \frac{\partial c}{\partial z}\right\} + S \quad (1)$$

where

c = is a scalar (e.g., salinity or concentration)
u, v, w = are the velocity components
D_x, D_y, D_z = are the directional dispersion coefficients
S = is a source or sink term
t = is the time
x, y, z = are the coordinates

It is assumed that the fluid is incompressible and that the flow field satisfies the continuity equation. Accordingly, equation (1) can be written as

$$\frac{\partial c}{\partial t} + u\frac{\partial c}{\partial x} + v\frac{\partial c}{\partial y} + w\frac{\partial c}{\partial z} = \frac{\partial}{\partial x}\left\{D_x \frac{\partial c}{\partial x}\right\} + \frac{\partial}{\partial y}\left\{D_y \frac{\partial c}{\partial y}\right\} + \frac{\partial}{\partial z}\left\{D_z \frac{\partial c}{\partial z}\right\} + S \quad (2)$$

To ensure mass conservation, it is natural to formulate the AD problem using a control volume approach (see *Figure 1*).

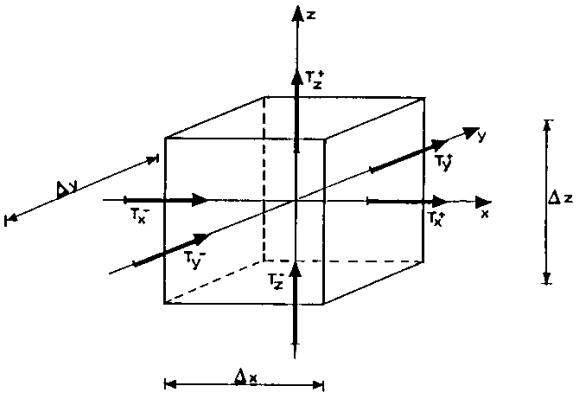

Figure 1. Control volume and definition of transports

In terms of transports (advective and dispersive) the advection-dispersion equation (1) simply states that the change in concentration is equal to the difference between the ingoing and outgoing transports plus the source-sink contribution. This can be written as an explicit scheme in finite difference form:

$$c^{n+1} = c^n - (T_x^+ - T_x^-) - (T_y^+ - T_y^-) - (T_z^+ - T_z^-) + S \quad (3)$$

A staggered computational grid is assumed in which the velocities are defined between the nodes and the concentrations at the nodes. The transport terms can then be written as

$$\begin{aligned}
T_x^+ &= T_x(j,k,l) = \sum_{i=1}^{8} (c_i^n \delta_i)_{j,k,l} \\
T_x^- &= T_x(j-1,k,l) = \sum_{i=1}^{8} (c_i^n \delta_i)_{j-1,k,l} \\
T_y^+ &= T_y(j,k,l) = \sum_{i=1}^{8} (c_i^n \gamma_i)_{j,k,l} \\
T_y^- &= T_y(j,k-1,l) = \sum_{i=1}^{8} (c_i^n \gamma_i)_{j,k-1,l} \\
T_z^+ &= T_z(j,k,l) = \sum_{i=1}^{8} (c_i^n \beta_i)_{j,k,l} \\
T_z^- &= T_z(j,k,l-1) = \sum_{i=1}^{8} (c_i^n \beta_i)_{j,k,l-1}
\end{aligned} \quad (4)$$

Here, c_i^n is the concentration at the nodes around the actual point, for example, (j, k, l), and δ_i, γ_i, β_i are discretization weights determined in such a way that the scheme becomes third-order accurate, thereby reducing numerical dispersion and wiggles. The locations of δ_i, γ_i, β_i can be seen in *Figure 2* for T_x^+, T_y^+, and T_z^+. The locations of δ_i, γ_i, β_i for T_x^-, T_y^-, and T_z^- are obtained by shifting the increments minus 1 for j, k, and l, respectively.

The derivation of the scheme follows Ekebjærg and

Advection-dispersion modelling: H. J. Vested et al.

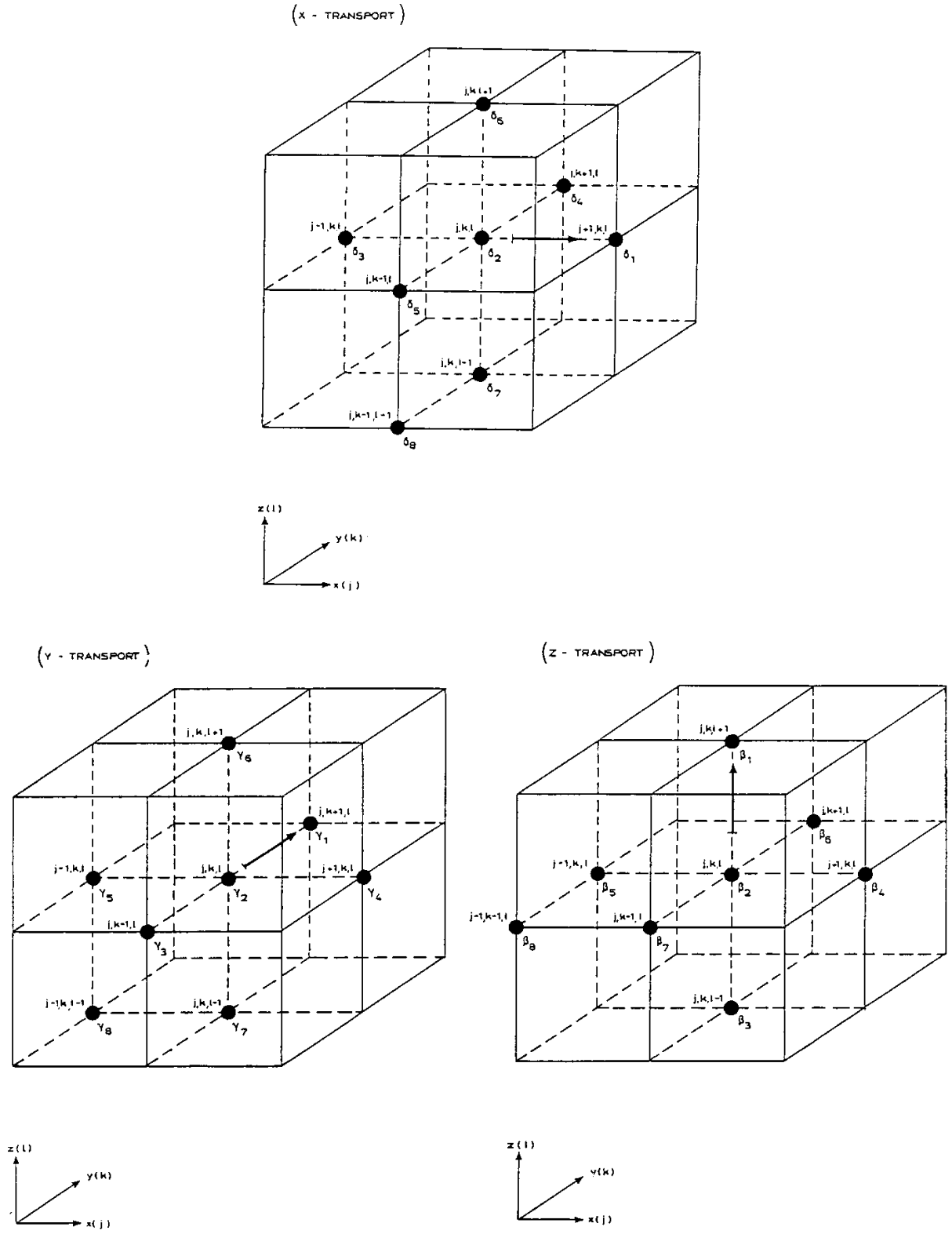

Figure 2. Locations of 3-D interpolation weights

Justesen.[9] A Taylor expansion of the time derivative in equation (2) gives (retaining terms of up to third order)

$$\frac{c^{n+1}_{j,k,l} - c^{n}_{j,k,l}}{\Delta t} + u\frac{\partial c}{\partial x} + v\frac{\partial c}{\partial y} + w\frac{\partial c}{\partial z} = D_x\frac{\partial^2 c}{\partial x^2} + D_y\frac{\partial^2 c}{\partial y^2} + D_z\frac{\partial^2 c}{\partial z^2} + \frac{1}{2}\Delta t\frac{\partial^2 c}{\partial t^2} + \frac{1}{6}\Delta t^2\frac{\partial^2 c}{\partial t^3} \quad (5)$$

Source-sink terms are omitted, and it is assumed that the dispersion tensor is constant. The new time derivatives are removed by differentiating the original equation (2) twice with respect to time and substituting it into (5). The flow field is assumed to be steady over the control volume. The convective terms are discretized by usual central differences, and all terms from the Taylor expansions up to third order are retained.

The next step is to discretize the remaining space derivatives, which is done by inserting Taylor expansions that are upstream centered and again retaining terms up to third order. It is convenient to introduce the Courant numbers $\sigma_x = u\Delta t/\Delta x$, $\sigma_y = v\Delta t/\Delta y$, $\sigma_z = w\Delta t/\Delta z$ and the dimensionless dispersion coefficients $\alpha_x = D_x\Delta t/\Delta x^2$, $\alpha_y = D_y\Delta t/\Delta y^2$, $\alpha_z = D_z\Delta t/\Delta z^2$.

The derivation of the scheme is from now on straightforward and requires only some algebraic effort (see the Appendix). The outcome is the discretization weights as functions of $(\sigma_x, \sigma_y, \sigma_z)$ and $(\alpha_x, \alpha_y, \alpha_z)$ as given in *Table 1*.

The locations of the weights are determined by the points that enter into the discretization and therefore have several possibilities. The locations of the weights as seen in *Figure 2* have been chosen. A scheme with ten weights has also been used but did not prove to be superior. It should be mentioned that, for example, node 8 is necessary for discretizing the term $\partial^3 c/\partial x\,\partial y\,\partial z$ and obtaining the correct solution for $\sigma_x = \sigma_y = \sigma_z = 1.0$.

Because the scheme is upstream centered, the weights are positioned relative to the actual direction of the flow, which is assumed to be in the positive direction of the coordinate systems shown in *Figure 2*. If the flow is in the negative direction, the locations of the weights shift accordingly. A numerical scheme that changes its form in this way with the flow is called a flow-adaptive numerical scheme.[12]

Of course, the explicit formulation of the scheme limits the possible time step length. However, this formulation has been preferred for two reasons. First, it facilitates a mass conservative formulation, and second, it gives a simple scheme to implement. An implicit scheme can be formulated by letting all spatial derivatives be located at the new time step. This leads to solving the full matrix equation. Another possibility could be to use the Thomas algorithm, solving the matrix equation iteratively. The benefits of such an approach and the consequence for the mass conservation will be documented later.

Stability analysis

To evaluate the application limits of the explicit finite difference scheme, a von Neumann stability analysis of the scheme has been carried out.

Consider the scheme in the Appendix, equation (A3). The solution is expanded as a Fourier series. The concentration at point (j, k, l) at time step n is written as

$$c^{n}_{j,k,l} = V^n \exp\{i(j\theta_x + k\theta_y + l\theta_z)\} \quad (6)$$

where i is the imaginary unit, θ_x, θ_y, and θ_z are the phase angles defined by

$$\theta_x = \frac{2\pi}{N_x}, \qquad \theta_y = \frac{2\pi}{N_y}, \qquad \theta_z = \frac{2\pi}{N_z} \quad (7)$$

and N_x, N_y, and N_z are the numbers of grid points per wavelength in the three directions. The amplification of c is described by a matrix G defined by

$$V^{n+1} = GV^n \quad (8)$$

which, for example, gives

$$c^{n+1}_{j+1,k,l} = GV^n \exp\{i(j+1)\theta_x + k\theta_y + l\theta_z)\} \quad (9)$$

This gives an equation for G by substituting into equation (A3). The necessary and sufficient condition for stability is then

$$|G| \le 1 \quad (10)$$

Examples of contour plots of $|G|$ for the highest resolvable wave ($N = 2$) as a function of σ_x and σ_y and for two values of σ_z, 0.25 and 0.5, are given below. The dimensionless dispersion is the same in all three directions, and three values are shown: $\alpha_x = \alpha_y = \alpha_z = 0.0$, 0.1, and 0.2. *Figures 3* and *4* reveal that an increasing Courant number decreases the stable region. Dispersion increases the stable region up to a certain limit, whereupon it restricts the stability again. Because an infinite number of combinations of $(\sigma_x, \sigma_y, \sigma_z)$ and $(\alpha_x, \alpha_y, \alpha_z)$ exists, the most convenient way to determine

Table 1. The weight functions

i	δ_i	γ_i	β_i
1	$\sigma_x(\frac{1}{6}\sigma_x^2 - \frac{1}{2}\sigma_x + \frac{1}{3} + \alpha_x) - \alpha_x$	$\sigma_y(\frac{1}{6}\sigma_y^2 - \frac{1}{2}\sigma_y + \frac{1}{3} + \alpha_y) - \alpha_y$	$\sigma_z(\frac{1}{6}\sigma_z^2 - \frac{1}{2}\sigma_z + \frac{1}{3} + \alpha_z) - \alpha_z$
2	$\sigma_x - \Sigma\delta_i,\ i \neq 2$	$\sigma_y - \Sigma\gamma_i,\ i \neq 2$	$\sigma_z - \Sigma\beta_i,\ i \neq 2$
3	$\sigma_x(-\frac{1}{6} + \frac{1}{6}\sigma_x^2 + \alpha_x)$	$\sigma_y(-\frac{1}{6} + \frac{1}{6}\sigma_y^2 + \alpha_y)$	$\sigma_z(-\frac{1}{6} + \frac{1}{6}\sigma_z^2 + \alpha_z)$
4	$\sigma_x(-\frac{1}{2}\sigma_y + \frac{1}{2}\sigma_y^2 + \alpha_y)$	$\sigma_y(-\frac{1}{2}\sigma_x + \frac{1}{2}\sigma_x^2 + \alpha_x)$	$\sigma_z(-\frac{1}{2}\sigma_x + \frac{1}{2}\sigma_x^2 + \alpha_x)$
5	$\sigma_x(\frac{1}{2}\sigma_x\sigma_y + \alpha_y - \frac{1}{3}\sigma_y\sigma_z)$	$\sigma_y(\frac{1}{2}\sigma_x\sigma_y + \alpha_x - \frac{1}{3}\sigma_x\sigma_z)$	$\sigma_x(\frac{1}{2}\sigma_x\sigma_z + \alpha_x - \frac{1}{3}\sigma_x\sigma_y)$
6	$\sigma_x(-\frac{1}{2}\sigma_z + \frac{1}{2}\sigma_z^2 + \alpha_z)$	$\sigma_y(-\frac{1}{2}\sigma_z + \frac{1}{2}\sigma_z^2 + \alpha_z)$	$\sigma_z(-\frac{1}{2}\sigma_y + \frac{1}{2}\sigma_y^2 + \alpha_y)$
7	$\sigma_x(\frac{1}{2}\sigma_x\sigma_z + \alpha_z - \frac{1}{3}\sigma_y\sigma_z)$	$\sigma_y(\frac{1}{2}\sigma_y\sigma_z + \alpha_z - \frac{1}{3}\sigma_x\sigma_z)$	$\sigma_z(\frac{1}{2}\sigma_y\sigma_z + \alpha_y - \frac{1}{3}\sigma_x\sigma_y)$
8	$\sigma_x(\frac{1}{3}\sigma_y\sigma_z)$	$\sigma_y(\frac{1}{3}\sigma_x\sigma_z)$	$\sigma_z(\frac{1}{3}\sigma_x\sigma_y)$

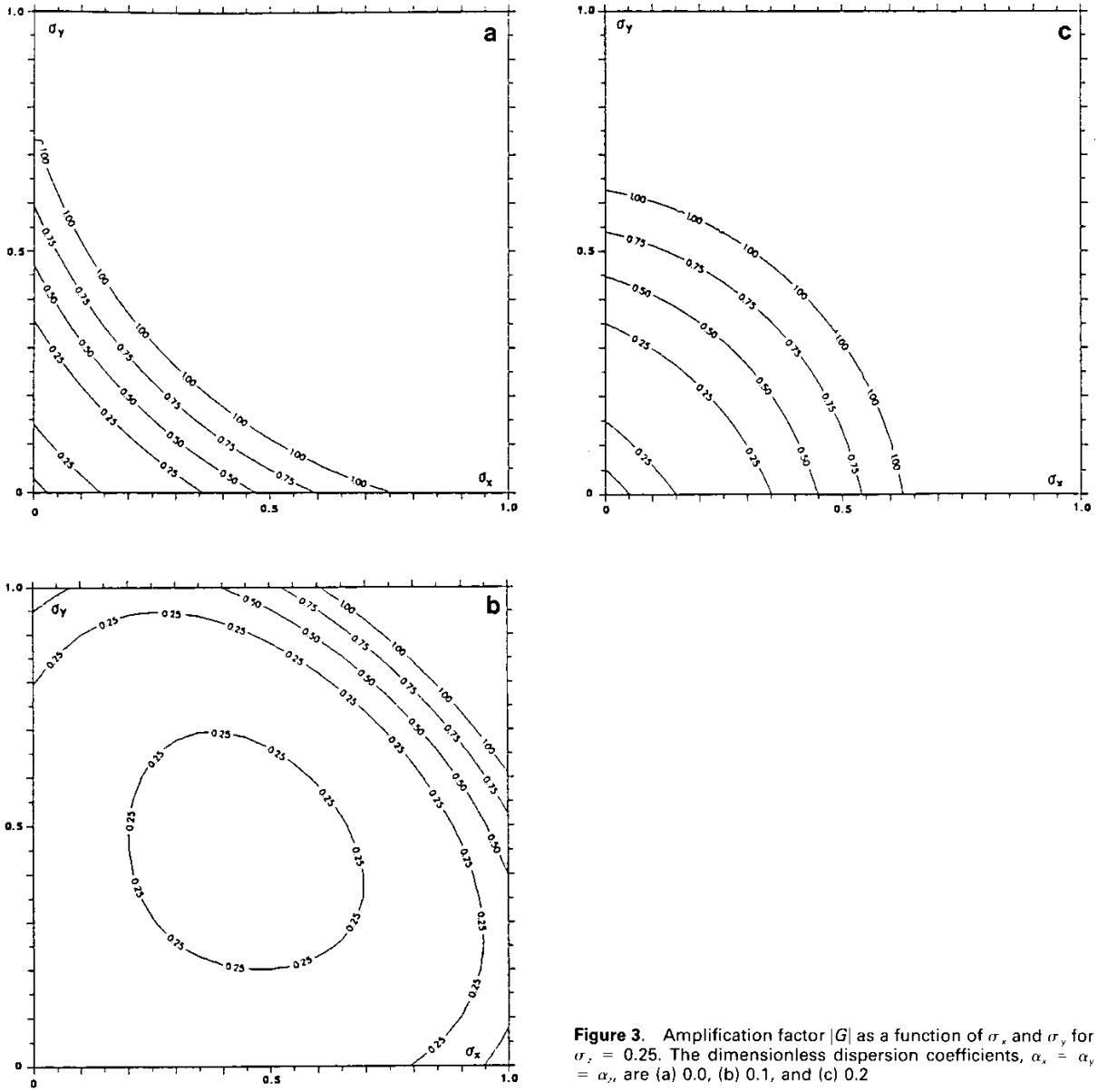

Figure 3. Amplification factor $|G|$ as a function of σ_x and σ_y for $\sigma_z = 0.25$. The dimensionless dispersion coefficients, $\alpha_x = \alpha_y = \alpha_z$, are (a) 0.0, (b) 0.1, and (c) 0.2

stability is actually by using the stability program interactively. For the applications of the scheme, stability has not been a problem for two reasons. For pure AD problems the velocity field is known *a priori* and the appropriate time step can be determined from the stability diagrams. When the model is coupled to an HD model, it is this model that will usually determine the largest possible time step.

It is interesting to note that for two dimensions the stability criterion is restricted by the straight line $\sigma_x + \sigma_y \leq 0.5$, whereas for three dimensions the stability surfaces are curved, and a stability criterion on the safe side is $\sigma_x + \sigma_y + \sigma_z \leq 0.8$. Both these stability limits are valid for the case of no dispersion.

Examples

Traditional two-dimensional benchmark tests, such as convected and rotated cones and a two-dimensional cavity flow, can be seen in Ref. 9. The present scheme becomes identical to their scheme if the z-plane is omitted. To illustrate the behavior of the present AD scheme, advection-dispersion of a 3-D Gaussian concentration field is presented below. This concentration

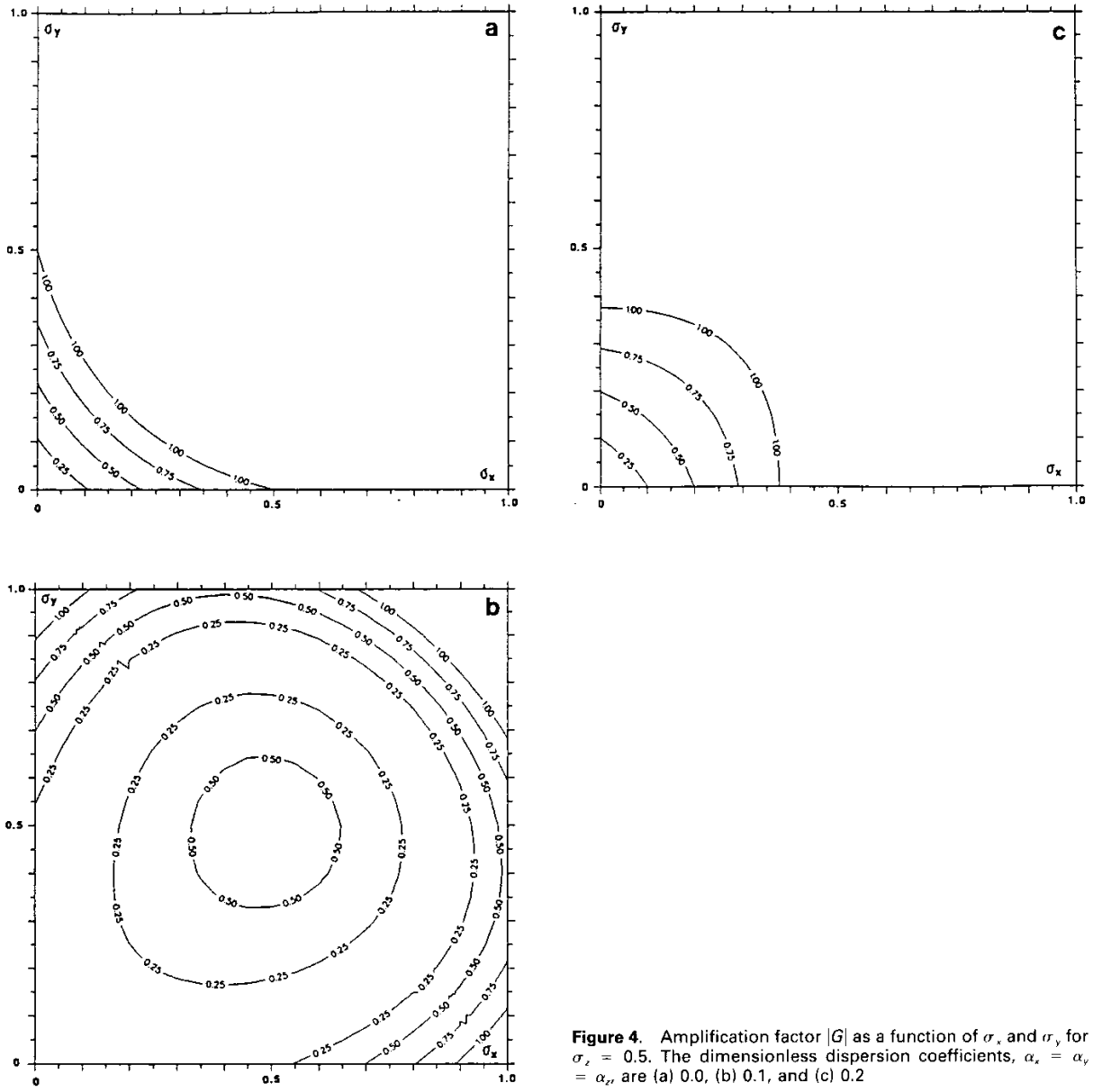

Figure 4. Amplification factor $|G|$ as a function of σ_x and σ_y for $\sigma_z = 0.5$. The dimensionless dispersion coefficients, $\alpha_x = \alpha_y = \alpha_z$, are (a) 0.0, (b) 0.1, and (c) 0.2

field represents an analytical solution to the AD equation for constant velocity field and dispersion coefficients.

Comparison with analytical results

The AD scheme has been tested in a square represented by 31 grid points in each direction, $\Delta x = \Delta y = \Delta z = 10$ m and $\Delta t = 5$ s. The grid dependence of the scheme is examined by varying the Courant numbers $\sigma_x, \sigma_y, \sigma_z$.

The initial Gaussian concentration field is written as

$$c(x, y, z) = \exp\left(-\frac{1}{2\delta_0^2}\left((x - x_0)^2 + (y - y_0)^2 + (z - z_0)^2\right)\right)$$

Advection-dispersion modelling: H. J. Vested et al.

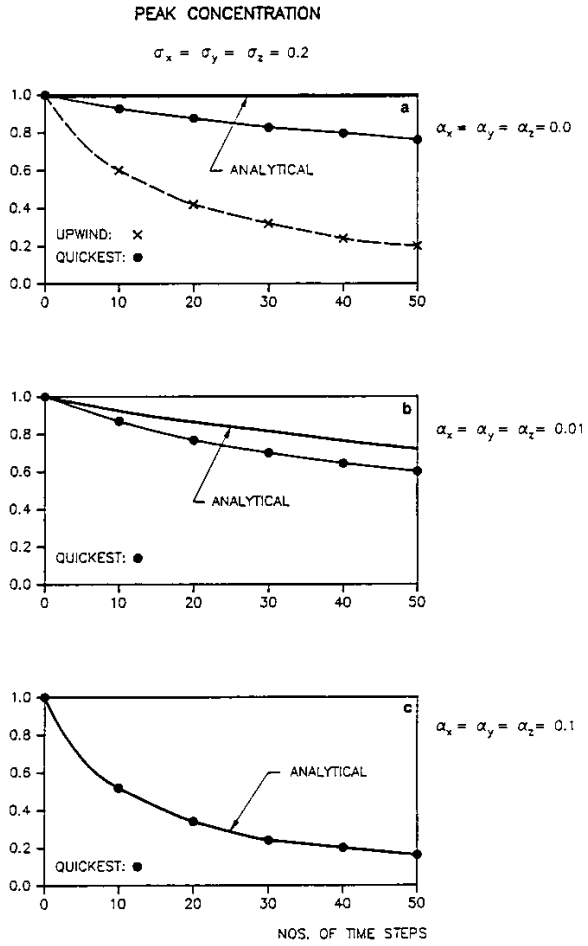

Figure 5. Advection-dispersion of a Gaussian sphere in a 3-D velocity field. Comparison between analytical calculated peak concentration and simulation. (a) No dispersion; (b) $\alpha_x = \alpha_y = \alpha_z = 0.01$; (c) $\alpha_x = \alpha_y = \alpha_z = 0.1$

where $(x_0, y_0, z_0) = (7\Delta x, 7\Delta y, 7\Delta z)$ is the center of gravity. The initial standard deviation δ_0 is equal to $2\Delta x$. This means that the width of the initial Gaussian field is approximately $12\Delta x$, that is, the concentration decays from unity of the center to about zero over six grid points.

First, the performance of the scheme is examined with a uniform velocity field, defined by $\sigma_x = \sigma_y = \sigma_z = 0.2$. *Figure 5* shows the peak concentrations through 50 computational steps and a comparison with the analytical solutions (the center of gravity is correctly advected in all cases and therefore is not shown). For the case with zero dispersion, $\alpha_x = \alpha_y = \alpha_z = 0.0$, the peak attenuates from 1.0 to 0.76 over the 50 time steps. Also shown are the results from using an explicit upwind scheme, reducing the peak to about 0.20. Adding a dispersion coefficient, as defined by setting $\alpha_x = \alpha_y = \alpha_z = 0.01$, reduces the relative error between the AD scheme and the analytical solution as expected. Increasing the dispersion coefficient further by a factor of ten leads to exact agreement with the analytical solution. A numerical experiment in which a negative dispersion equal to $\alpha_x = \alpha_y = \alpha_z = -0.01$ has been used leads to almost exact performance of the scheme (the actual values deviated by 1–2 percent). This indicates for these conditions an inherent numerical dispersion of about 0.01 in dimensionless terms.

Changing the Courant numbers to investigate the grid dependence of the scheme is visualized in *Figure 6* for the case with zero dispersion. It is seen that the numerical dispersion does not change for lower Courant numbers or advection at a skew angle.

Comparison with other schemes

As was mentioned above, *Figure 5* shows a comparison between the QUICKEST scheme and the simple first-order explicit upwind scheme. The inherent numerical dispersion of the upwind scheme can be evaluated as $D_{\text{num},x} = u\Delta x(1 - \sigma_x)/2 = 0.4 \cdot 1.0 \cdot (1 - 0.2)/2 = 1.6$ or $\alpha_x = 0.08$. An extension to three dimensions of the Lax-Wendroff scheme was also examined. This is a descent from the QUICKEST scheme in which all third-order correction terms are omitted. This scheme gave slightly less attenuation of the peak value (0.80 after 50 time steps); but the concentration field did not remain symmetrical, and the center of gravity was not correctly advected.

To further illustrate the use of QUICKEST with

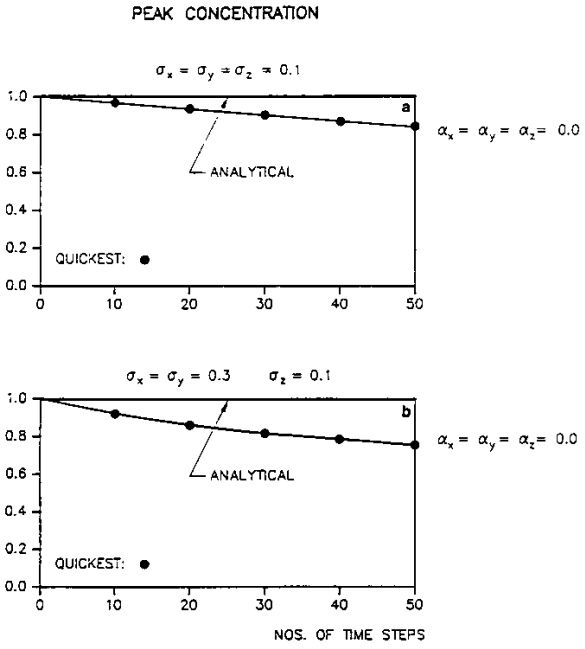

Figure 6. Advection-dispersion of a Gaussian sphere in a 3-D velocity field. Comparison between analytical calculated peak concentrations and simulation. (a) Reduced Courant numbers, $\sigma_x = \sigma_y = \sigma_z = 0.1$; (b) advection at a skew angle, $\sigma_x = \sigma_y = 0.3$, $\sigma_z = 0.1$

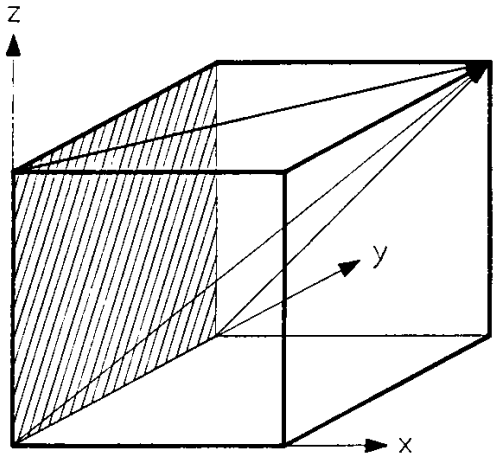

Figure 7. Sketch of a theoretical concentration field in a 3-D scalar test

respect to numerical dispersion, the classical cross-flow of scalar transport[10] has been extended to a 3-D problem. Consider a cube with uniform flow along the diagonal from the front lower left corner to the upper right back corner, with the left wall boundary value equal to unity and all other boundary values being zero. The steady solution with no dispersion is a concentration equal to unity along the direction of the streamlines as sketched in *Figure 7*. *Table 2* lists the steady-state values as calculated by the 3-D scheme described by Patankar[10] (implicit upwind scheme) and QUICKEST through a forward time stepping. The computational setup is equal to the one described above, but for reasons of clarity, only a 10 × 10 grid point subset of horizontal plane 10 is given. It is seen that the QUICKEST scheme resolves the front more correctly, though not without minor wiggles close to the front. The donor cell scheme or upwind scheme is, of course, more dispersive. This is in agreement with Patankar,[10] who states that reduction of the numerical dispersion can be obtained by aligning the numerical mesh with the flow direction or by involving more points in the numerical scheme.

A very severe 3-D test case is reported by Smolarkiewicz.[11] Consider a computational box with the dimensions of 41 × 41 × 41 grid points, $\Delta x = \Delta y = \Delta z = 2.5$ m, and a constant angular velocity $\Omega = (\omega/2, \omega/2, \omega/\sqrt{2})$, where $\omega = 0.1\ s^{-1}$.

The velocity components are $u = -\Omega_1(y - y_0) + \Omega_2(z - z_0)$, $v = -\Omega_3(x - x_0) - \Omega_1(z - z_0)$, $w = -\Omega_2(x - x_0) + \Omega_1(y - y_0)$, where $(x_0, y_0, z_0) = (20\Delta x, 20\Delta y, 20\Delta z)$. The initial condition was a sphere with a radius of $7\Delta x$ and a linearly variable density from zero at the edge to four at the center $(20\Delta x - 7\Delta x\sqrt{6}, 20\Delta x - 7\Delta x\sqrt{6}, 20\Delta x + 14\Delta x\sqrt{6})$. The sphere is rotating around the diagonal axis of the box.

The time step was equal to 0.1 s, and a full revolution takes 628 time steps. Smolarkiewicz used this test, which is an extension to three dimensions of the traditional rotating cone test, for evaluating his positive definite advection scheme (so-called four-point iteration scheme).

Table 3 shows a comparison of the maximum values and the variance error (ER2) between start and end after five revolutions as given by Smolarkiewicz[11] and as calculated with the present scheme.

From *Table 3* it can be seen that QUICKEST performs approximately as well as the third-order-accurate version of the four-point iteration scheme and, as expected, better than the second-order scheme. *Figure 8* shows a subset of the computational box visualizing the initial concentration field and the concentration field after five revolutions. It is seen that the field remains symmetrical, though with a slight tendency to elongate toward the center of rotation.

Coupling to a hydrodynamic model (lock exchange flow)

The AD scheme can be coupled to a hydrodynamic (HD) model. With an initial density distribution the HD model solves the momentum and continuity equations, giving a velocity field that is used as input to the AD

Table 3. Comparison between the results of Smolarkiewicz[11] and QUICKEST for a 3-D rotating sphere

	Maximum value	ER2
Smolarkiewicz		
Second-order accurate	1.67	0.63
Third-order accurate	2.69	0.54
QUICKEST	2.32	0.32

Table 2. Comparison of the steady-state upwind scheme of Patankar[10] and the QUICKEST scheme for a three-dimensional scalar test. Horizontal plane 10

Upwind	QUICKEST
1.00 1.00 0.98 0.95 0.90 0.82 0.71 0.60 0.48 0.38	1.00 1.00 1.00 1.01 1.03 1.05 1.01 0.88 0.67 0.43
1.00 1.00 0.98 0.93 0.86 0.76 0.65 0.53 0.42 0.31	1.00 1.00 1.00 1.02 1.04 1.02 0.92 0.73 0.49 0.27
1.00 0.99 0.96 0.90 0.81 0.69 0.57 0.45 0.34 0.25	1.00 1.00 1.01 1.03 1.01 0.93 0.75 0.51 0.28 0.11
1.00 0.98 0.93 0.85 0.73 0.60 0.47 0.35 0.26 0.18	1.00 1.01 1.02 1.01 0.93 0.75 0.51 0.28 0.11 0.01
1.00 0.97 0.89 0.77 0.63 0.49 0.36 0.26 0.17 0.12	1.00 1.01 1.02 0.94 0.76 0.51 0.27 0.10 0.00 -.03
1.00 0.94 0.81 0.65 0.50 0.36 0.25 0.16 0.10 0.07	1.00 1.01 0.96 0.77 0.51 0.26 0.08 -.01 -.03 -.02
1.00 0.87 0.69 0.50 0.34 0.22 0.14 0.09 0.05 0.03	1.00 0.98 0.80 0.51 0.24 0.07 -.01 -.03 -.02 -.01
1.00 0.75 0.50 0.31 0.19 0.11 0.06 0.03 0.02 0.01	1.00 0.84 0.51 0.22 0.05 -.01 -.02 -.01 0.00 0.00
1.00 0.50 0.25 0.12 0.06 0.03 0.02 0.01 0.00 0.00	1.00 0.51 0.18 0.03 -.01 -.01 -.01 0.00 0.00 0.00
0.00 0.00 0.00 0.00 0.00 0.00 0.00 0.00 0.00 0.00	0.00 0.00 0.00 0.00 0.00 0.00 0.00 0.00 0.00 0.00

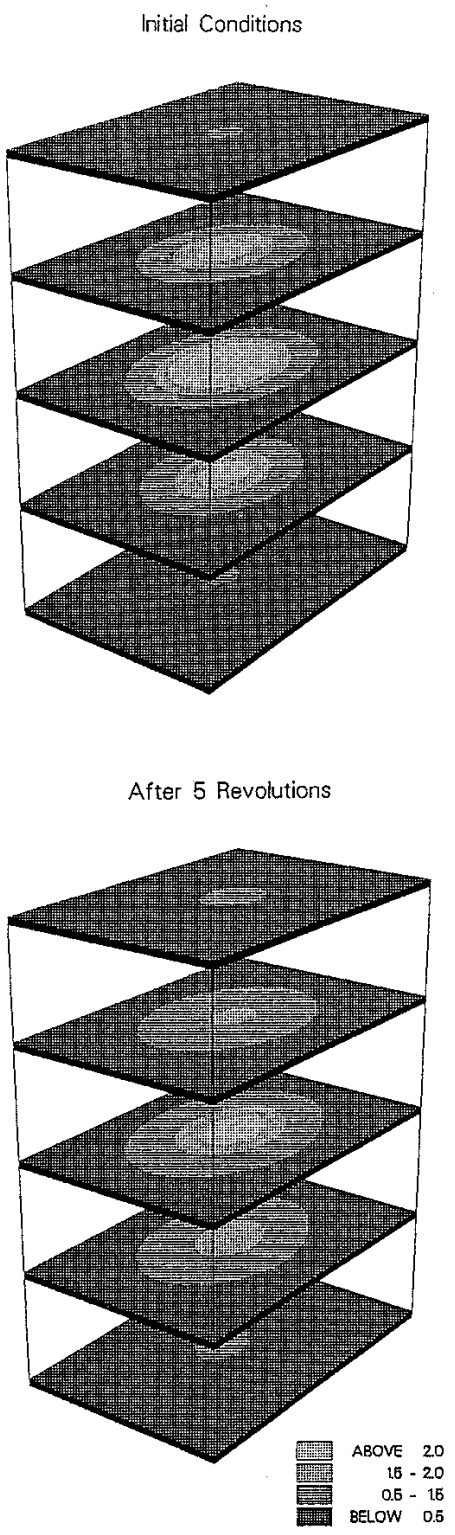

Figure 8. Subset of the computational box, visualizing the initial and final concentration field after five revolutions, for the 3-D rotating sphere test

scheme to find the new density distribution, and so the HD model can proceed. The HD model used is described by Rasmussen et al.[13]

As an example of a coupled HD-AD simulation, the classical lock exchange flow has been simulated in order to examine the performance of the AD scheme. The flow is two-dimensional in the *xz*-plane. Initially, the water is at rest, with the less dense water to the left and the more dense water to the right. When the wall is suddenly removed, the stratification is, of course, unstable, and the two water bodies will start to move.

To simulate the flow correctly, the density front must remain sharp. Heavy numerical dispersion would smooth out the front, the flow would cease, and numerical wiggles could cause nonphysical density gradients. A test rig was set up defined by 20 × 40 grid points in the vertical and horizontal directions, respectively. The vertical grid size was 1.0 m, and the horizontal grid size was 100 m. The time step was 2.5 s.

Figure 9 shows the temporal development in the flow after 0, 600, and 1200 time steps. The initial front is three grid spacings wide, and the actual density varies in terms of salinity from 20 to 32. The presented results are computed with pure advection.

It can be seen that the flow is symmetrical, as expected. The front is smoothed at the start of the simulation and then remains unchanged, even though the velocity field is very complicated and unsteady. The maximum Courant numbers are about 0.02, so there are no stability problems. (In the present case the time step is determined by the HD model.)

There are, of course, also wiggles at the front providing variations of up to 10 percent of the maximum salinity difference, but these are apparently not large enough to influence the main flow features.

For a further discussion of the simulation of the lock exchange flow and comparison with measurements, see Ref. 14.

Application in groundwater flow

The AD scheme has also been used for simulating dispersion in groundwater by coupling it to a 3-D groundwater flow model.[15] This model complex has been applied as a part of a natural gradient dispersion test in a sandy aquifer using tritium as a tracer.[16] Tritium was injected as a slug, and the advection and dispersion of the plume were monitored by water sampling in a dense three-dimensional mesh of piezometers, making a comparison between model results and measurements possible. The grid spacing was 1.0 m in the horizontal model and 0.5 m in the vertical. There were 220 × 30 cells in the horizontal and nine levels in the vertical. The time step for the AD scheme was approximately 7 hours, restricted by the stability criteria. The simulation period was about 6 months.

In *Figure 10* a comparison is shown between measured and calculated tritium concentrations taken from Ref. 16. The upper part of the figure presents contour plots of the vertically and horizontally averaged tritium concentrations at different times after injection. The

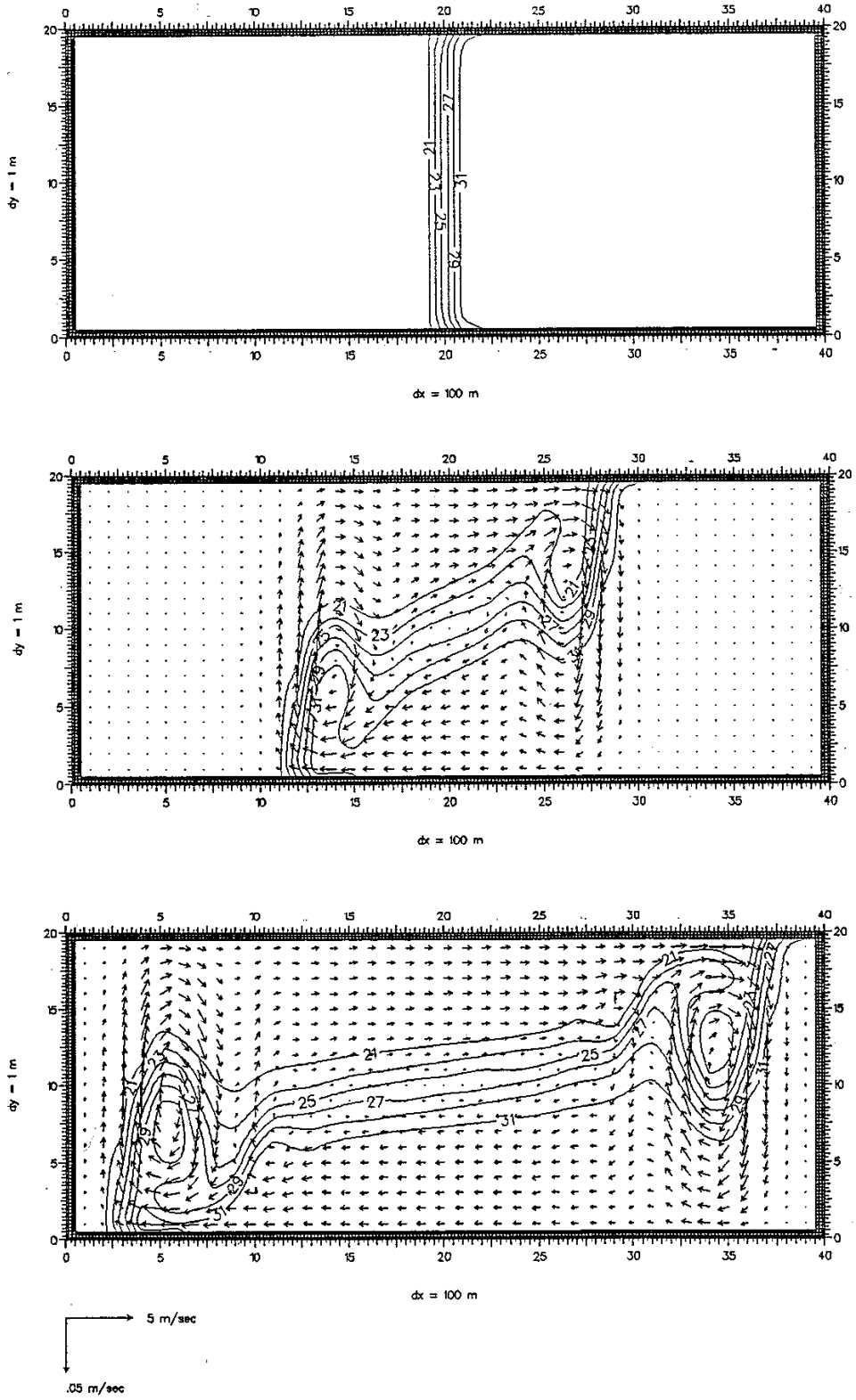

Figure 9. Lock exchange flow. (a), (b), and (c) are time steps 0, 600, and 1200, respectively. The plotted contours are isolines of salinity

Advection-dispersion modelling: H. J. Vested et al.

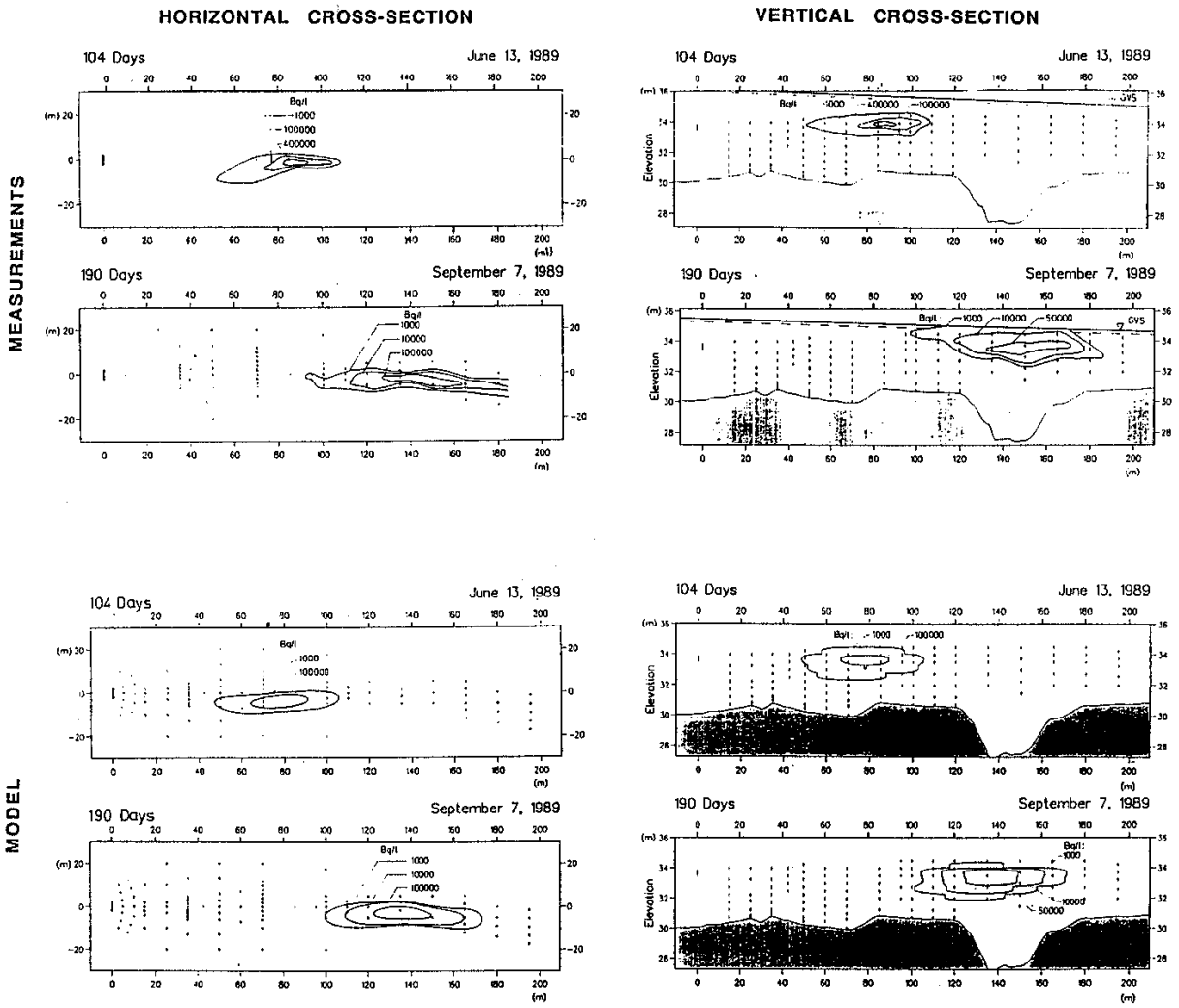

Figure 10. Groundwater flow. Vertically and horizontally integrated concentration field. Upper part: measured values; lower part: simulated values[16]

corresponding simulated results are shown below. It is seen that there is good agreement between measurements and calculations regarding travel velocity and spreading in horizontal and vertical directions. The interesting point in this study was that the model dispersion coefficients that gave the best comparison with the measured concentration fields are also comparable to the actually measured dispersion coefficients.

Conclusion

The explicit finite difference scheme QUICKEST for solving advection-dispersion problems has been extended to three dimensions. A control volume formulation is used to ensure mass conservation. The scheme, which is accurate up to third order, limits the problems of numerical wiggles and dispersion such as are known from central differencing of upwind schemes and is therefore well suited for coupling to a hydrodynamic model, thus simulating flow problems in which density gradients are of importance. This is due to the rather simple and thereby cost-effective formulation of the scheme together with a minimum of numerical diffusion and wiggles at fronts. The scheme admittedly suffers from some wiggling at steep fronts. In the intended area of applications, which are turbulent flow in seas and groundwater flow, some dispersion is always present, thus reducing the problem. However, the methodology of using a bounded exponential interpolation in regions with steep fronts, as described by Leonard,[7] is under consideration.

The scheme being explicit necessitates a stability analysis, and diagrams have been prepared to determine computationally stable regions.

Acknowledgments

The authors would like to thank Professor M. B. Abbott of the International Institute for Hydraulic Engineering, Delft, and their colleagues at the Danish Hydraulic Institute, E. B. Rasmussen, K. W. Olesen, and I. R. Warren, for inspiration and their help with carrying out the presented work. Also thanks to our colleagues in the field of groundwater flow for lending us their results.

The work has been supported by the Danish Technical Research Council.

References

1 Bode, L. and Sobey, R. J. Accurate modelling of two-dimensional mass transport. *Proceedings of the 19th International Conference on Coastal Engineering*, ASCE, Houston, 1984, pp. 2434–2448
2 Zalesak, S. T. Fully multi-dimensional flux-corrected transport algorithms for fluids. *J. Comput. Phys.* 1979, **31,** 335–362
3 Leonard, B. P. A stable and accurate convective modelling procedure based on quadratic upstream interpolation. *Comput. Methods Appl. Mech. Engrg.* 1979, **19,** 59–98
4 Davis, R. W. and Moore, E. F. A numerical study of vortex shedding from rectangles. *J. Fluid Mech.* 1982, **116,** 475–506
5 ASCE. Turbulence modelling of surface water flow and transport: Parts I–V. *J. Hydraulic Engrg.* 1988, **114**(9), 970–1073
6 Abbott, M. B. and Basco, D. R. *Computational Fluid Dynamics: An Introduction for Engineers.* Longman, London; Wiley, New York, 1989
7 Leonard, B. P. Simple high-accuracy resolution program for convective modelling of discontinuities. *Internat. J. Numer. Methods Fluids.* 1988, **8,** 1291–1318
8 Justesen, J., Olesen, K. W., and Vested, H. J. High accuracy modelling of advection in two and three dimensions. *Proceedings of the 23rd IAHR Congress*, Ottawa, Canada, 1989, pp. D239–246
9 Ekebjærg, L. and Justesen, P. An explicit scheme for advection-diffusion modelling in two dimensions. *Comput. Methods Appl. Mech. Engrg.* 1991, **88,** 287–297
10 Patankar, S. V. *Numerical Heat Transfer and Fluid Flow.* Series in Computational Methods in Mechanical and Thermal Sciences. McGraw-Hill, New York, 1980
11 Smolarkiewicz, P. K. A fully multidimensional positive definite advection transport algorithm with small implicit diffusion. *J. Comput. Phys.* 1984, **54,** 325–362
12 Abbott, M. B., Havnø, K., and Lindberg, S. The fourth generation of numerical modelling in hydraulics. *J. Hydraul. Res.* 1991, **29**(5), 581–600
13 Rasmussen, E. B., Vested, H. J., Justesen, P., and Ekebjærg, L. *SYSTEM3 Final Report.* Danish Hydraulic Institute, Hørsholm, Denmark, 1990
14 Rasmussen, E. B., Vested, H. J., and Ekebjærg, L. Numerical 3-D current modelling of stratified seas. *International Conference on Coastal Engineering*, The Netherlands, 1990, Chapter 89, p. 1186
15 Refsgaard, A., Refsgård, J. C., and Clausen, T. Three dimensional modelling of groundwater flow and solute transport. To be submitted to *Journal of Contaminant Transport*, 1991
16 Høgh Jensen, K., Bitsch, K., and Bjerg, P. L. Large scale experiment in a sandy aquifier in DK: observed tracer movement and numerical analyses. Institute of Hydrodynamics and Hydraulic Engineering (ISVA), Technical University of Denmark, submitted

Appendix: Derivation of the scheme

Taking the starting point in equation (5), where the second and third derivatives in time are removed by differentiating the original equation (2) twice with respect to time and discretizing the convective terms by usual control differences lead to equation (A1), in which all the terms from the Taylor expressions up to third order have been retained:

$$\begin{aligned}
&\frac{c^{n+1}_{j,k,l} - c^{n}_{j,k,l}}{\Delta t} + u\frac{c^{n}_{j+1,k,l} - c^{n}_{j-1,k,l}}{2\Delta x} + v\frac{c^{n}_{j,k+1,l} - c^{n}_{j,k-1,l}}{2\Delta y} + w\frac{c^{n}_{j,k,l+1} - c^{n}_{j,k,l-1}}{2\Delta z} \\
&= \left(D_x + \frac{1}{2}\Delta t u^2\right)\frac{\partial^2 c}{\partial x^2} + \left(D_y + \frac{1}{2}\Delta t v^2\right)\frac{\partial^2 c}{\partial y^2} + \left(D_z + \frac{1}{2}\Delta t w^2\right)\frac{\partial^2 c}{\partial z^2} + \Delta t uv\,\frac{\partial^2 c}{\partial x \partial y} + \Delta t uw\frac{\partial^2 c}{\partial x \partial z} + \Delta t vw\frac{\partial^2 c}{\partial y \partial z} \\
&\quad + \frac{1}{2}u\left(\frac{1}{3}\Delta x^2 - 2D_x\Delta t - \frac{1}{3}\Delta t^2 u^2\right)\frac{\partial^3 c}{\partial x^3} + \frac{1}{2}v\left(\frac{1}{3}\Delta y^2 - 2D_y\Delta t - \frac{1}{3}\Delta t^2 v^2\right)\frac{\partial^3 c}{\partial y^3} \\
&\quad + \frac{1}{2}w\left(\frac{1}{3}\Delta z^2 - 2D_z\Delta t - \frac{1}{3}\Delta t^2 w^2\right)\frac{\partial^3 c}{\partial z^3} + \frac{1}{2}v\Delta t(-u^2\Delta t - 2D_x)\frac{\partial^3 c}{\partial x^2 \partial z} + \frac{1}{2}w\Delta t(-v^2\Delta t - 2D_y)\frac{\partial^3 c}{\partial y^2 \partial z} \\
&\quad + \frac{1}{2}w\Delta t(-u^2\Delta t - 2D_x)\frac{\partial^3 c}{\partial x^2 \partial z} + \frac{1}{2}v\Delta t(-w^2\Delta t - 2D_z)\frac{\partial^3 c}{\partial z^2 \partial y} + \frac{1}{2}u\Delta t(-w^2\Delta t - 2D_z)\frac{\partial^3 c}{\partial z^2 \partial x} \\
&\quad + \frac{1}{2}u\Delta t(-v^2\Delta t - 2D_y)\frac{\partial^3 c}{\partial y^2 \partial y} - \Delta t^2 uv w\frac{\partial^3 c}{\partial x \partial y \partial z}
\end{aligned} \tag{A1}$$

The next step is to discretize the remaining space derivatives, which is done by inserting Taylor expansions that are upstream centered and again retaining terms up to third order. The Courant numbers $\sigma_x = u\Delta t/\Delta x$, $\sigma_y = v\Delta t/\Delta y$, $\sigma_z = w\Delta t/\Delta z$, and the dimensionless dispersion coefficients $\alpha_x = D_x\Delta t/\Delta x^2$, $\alpha_y = D_y\Delta t/\Delta y^2$, $\alpha_z = D_z\Delta t/\Delta z^2$ are introduced:

$$\begin{aligned}
&c^{n+1}_{j,k,l} - c^{n}_{j,k,l} + \tfrac{1}{2}\sigma_x(c^{n}_{j+1,k,l} - c^{n}_{j-1,k,l}) + \tfrac{1}{2}\sigma_y(c^{n}_{j,k+1,l} - c^{n}_{j,k-1,l}) + \tfrac{1}{2}\sigma_z(c^{n}_{j,k,l+1} - c^{n}_{j,k,l-1}) \\
&\quad = (\alpha_x + \tfrac{1}{2}\sigma_x^2)(c_{j-1,k,l} - 2c_{j,k,l} + c_{j+1,k,l}) + (\alpha_y + \tfrac{1}{2}\sigma_y^2)(c_{j,k-1,l} - 2c_{j,k,l} + c_{j,k+1,l}) \\
&\quad\quad + (\alpha_z + \tfrac{1}{2}\sigma_z^2)(c_{j,k,l-1} - 2c_{j,k,l} + c_{j,k,l+1}) + \sigma_x\sigma_y(c_{j,k,l} - c_{j-1,k,l} - c_{j,k-1,l} + c_{j-1,k-1,l})
\end{aligned}$$

Advection-dispersion modelling: H. J. Vested et al.

$$
\begin{aligned}
&+ \sigma_x\sigma_z(c_{j,k,l} - c_{j-1,k,l} - c_{j,k,l-1} + c_{j-1,k,l-1}) + \sigma_y\sigma_z(c_{j,k,l} - c_{j,k-1,l} - c_{j,k,l-1} + c_{j,k-1,l-1})\\
&+ \tfrac{1}{2}\sigma_x(\tfrac{1}{3} - 2\alpha_x - \tfrac{1}{3}\sigma_x^2)(c_{j+1,k,l} - 3c_{j,k,l} + 3c_{j-1,k,l} - c_{j-2,k,l})\\
&+ \tfrac{1}{2}\sigma_y(\tfrac{1}{3} - 2\alpha_y - \tfrac{1}{3}\sigma_y^2)(c_{j,k+1,l} - 3c_{j,k,l} + 3c_{j,k-1,l} - c_{j,k-2,l})\\
&+ \tfrac{1}{2}\sigma_z(\tfrac{1}{3} - 2\alpha_z - \tfrac{1}{3}\sigma_z^2)(c_{j,k,l+1} - 3c_{j,k,l} + 3c_{j,k,l-1} - c_{j,k,l-2})\\
&+ \tfrac{1}{2}\sigma_y(-\sigma_x^2 - 2\alpha_x + \sigma_x)(c_{j-1,k,l} - 2c_{j,k,l} + c_{j+1,k,l} - c_{j+1,k-1,l} + 2c_{j,k-1,l} - c_{j-1,k-1,l})\\
&+ \tfrac{1}{2}\sigma_z(-\sigma_y^2 - 2\alpha_y + \sigma_y)(c_{j,k-1,l} - 2c_{j,k,l} + c_{j,k+1,l} - c_{j,k+1,l} + 2c_{j,k,l-1} - c_{j,k-1,l-1})\\
&+ \tfrac{1}{2}\sigma_z(-\sigma_x^2 - 2\alpha_x + \sigma_x)(c_{j-1,k,l} - 2c_{j,k,l} + c_{j+1,k,l} - c_{j+1,k,l-1} + 2c_{j,k,l-1} - c_{j-1,k,l-1})\\
&+ \tfrac{1}{2}\sigma_y(-\sigma_z^2 - 2\alpha_z + \sigma_z)(c_{j,k,l-1} - 2c_{j,k,l} + c_{j,k,l+1} - c_{j,k-1,l+1} + 2c_{j,k-1,l} - c_{j,k-1,l-1})\\
&+ \tfrac{1}{2}\sigma_x(-\sigma_z^2 - 2\alpha_z + \sigma_z)(c_{j,k,l-1} - 2c_{j,k,l} + c_{j,k,l+1} - c_{j-1,k,l+1} + 2c_{j-1,k,l} - c_{j-1,k,l-1})\\
&+ \tfrac{1}{2}\sigma_x(-\sigma_y^2 - 2\alpha_y + \sigma_y)(c_{j,k-1,l} - 2c_{j,k,l} + c_{j,k+1,l} - c_{j-1,k+1,l} + 2c_{j-1,k,l} - c_{j-1,k-1,l})\\
&+ \sigma_x\sigma_y\sigma_z(-c_{j-1,k-1,l} - c_{j-1,k,l-1} - c_{j,k-1,l-1} + c_{j-1,k,l} + c_{j,k-1,l}\\
&+ c_{j,k,l-1} - c_{j,k,l} + c_{j-1,k-1,l-1}) \qquad \text{(A2)}
\end{aligned}
$$

Equation (A2) is then reorganized after the discretized values as shown below:

$$
\begin{aligned}
c_{j,k,l}^{n+1} = {} & c_{j,k,l}^{n}\{1 - 2(\alpha_x + \tfrac{1}{2}\sigma_x^2) - 2(\alpha_y + \tfrac{1}{2}\sigma_y^2) - 2(\alpha_z + \tfrac{1}{2}\sigma_z^2) + \sigma_x\sigma_y + \sigma_x\sigma_z + \sigma_y\sigma_z\\
&- \tfrac{3}{2}\sigma_x(\tfrac{1}{3} - 2\alpha_x - \tfrac{1}{3}\sigma_x^2) - \tfrac{3}{2}\sigma_y(\tfrac{1}{3} - 2\alpha_y - \tfrac{1}{3}\sigma_y^2) - \tfrac{3}{2}\sigma_z(\tfrac{1}{3} - 2\alpha_z - \tfrac{1}{3}\sigma_z^2)\\
&- \sigma_y(-\sigma_x^2 - 2\alpha_x + \sigma_x) - \sigma_z(-\sigma_y^2 - 2\alpha_y + \sigma_y) - \sigma_z(-\sigma_x^2 - 2\alpha_x + \sigma_x)\\
&- \sigma_y(-\sigma_z^2 - 2\alpha_z + \sigma_z) - \sigma_x(-\sigma_z^2 - 2\alpha_z + \sigma_z) - \sigma_x(-\sigma_y^2 - 2\alpha_y + \sigma_y) - \sigma_x\sigma_y\sigma_z\}\\
&+ c_{j+1,k,l}^{n}\{-\tfrac{1}{2}\sigma_x + (\alpha_x + \tfrac{1}{2}\sigma_x^2) + \tfrac{1}{2}\sigma_x(\tfrac{1}{3} - 2\alpha_x - \tfrac{1}{3}\sigma_x^2) + \tfrac{1}{2}\sigma_y(-\sigma_x^2 - 2\alpha_x + \sigma_x)\\
&\quad + \tfrac{1}{2}\sigma_z(-\sigma_x^2 - 2\alpha_x + \sigma_x)\}\\
&+ c_{j,k+1,l}^{n}\{-\tfrac{1}{2}\sigma_y + (\alpha_y + \tfrac{1}{2}\sigma_y^2) + \tfrac{1}{2}\sigma_y(\tfrac{1}{3} - 2\alpha_y - \tfrac{1}{3}\sigma_y^2) + \tfrac{1}{2}\sigma_z(-\sigma_y^2 - 2\alpha_y + \sigma_y)\\
&\quad + \tfrac{1}{2}\sigma_x(-\sigma_y^2 - 2\alpha_y + \sigma_y)\}\\
&+ c_{j,k,l+1}^{n}\{-\tfrac{1}{2}\sigma_z + (\alpha_z + \tfrac{1}{2}\sigma_z^2) + \tfrac{1}{2}\sigma_z(\tfrac{1}{3} - 2\alpha_z - \tfrac{1}{3}\sigma_z^2) + \tfrac{1}{2}\sigma_y(-\sigma_z^2 - 2\alpha_z + \sigma_z)\\
&\quad + \tfrac{1}{2}\sigma_x(-\sigma_z^2 - 2\alpha_z + \sigma_z)\}\\
&+ c_{j-1,k,l}^{n}\{\tfrac{1}{2}\sigma_x + (\alpha_x + \tfrac{1}{2}\sigma_x^2) - \sigma_x\sigma_y - \sigma_x\sigma_z + \tfrac{3}{2}\sigma_x(\tfrac{1}{3} - 2\alpha_x - \tfrac{1}{3}\sigma_x^2) + \tfrac{1}{2}\sigma_y(-\sigma_x^2 - 2\alpha_x + \sigma_x)\\
&\quad + \tfrac{1}{2}\sigma_z(-\sigma_x^2 - 2\alpha_x + \sigma_x) + \sigma_x(-\sigma_z^2 - 2\alpha_z + \sigma_z) + \sigma_x(-\sigma_y^2 - 2\alpha_y + \sigma_y) + \sigma_x\sigma_y\sigma_z\}\\
&+ c_{j,k-1,l}^{n}\{\tfrac{1}{2}\sigma_y + (\alpha_y + \tfrac{1}{2}\sigma_y^2) - \sigma_x\sigma_y - \sigma_y\sigma_z + \tfrac{3}{2}\sigma_y(\tfrac{1}{3} - 2\alpha_y - \tfrac{1}{3}\sigma_y^2) + \sigma_y(-\sigma_x^2 - 2\alpha_x + \sigma_x)\\
&\quad + \tfrac{1}{2}\sigma_z(-\sigma_y^2 - 2\alpha_y + \sigma_y) + \sigma_y(-\sigma_z^2 - 2\alpha_z + \sigma_z) + \tfrac{1}{2}\sigma_x(-\sigma_y^2 - 2\alpha_y + \sigma_y) + \sigma_x\sigma_y\sigma_z\}\\
&+ c_{j,k,l-1}^{n}\{\tfrac{1}{2}\sigma_z + (\alpha_z + \tfrac{1}{2}\sigma_z^2) - \sigma_x\sigma_z - \sigma_y\sigma_z + \tfrac{3}{2}\sigma_z(\tfrac{1}{3} - 2\alpha_z - \tfrac{1}{3}\sigma_z^2) + \sigma_z(-\sigma_y^2 - 2\alpha_y + \sigma_y)\\
&\quad + \sigma_z(-\sigma_x^2 - 2\alpha_x + \sigma_x) + \tfrac{1}{2}\sigma_y(-\sigma_z^2 - 2\alpha_z + \sigma_z) + \tfrac{1}{2}\sigma_x(-\sigma_z^2 - 2\alpha_z + \sigma_z) + \sigma_x\sigma_y\sigma_z\}\\
&+ c_{j-2,k,l}^{n}\{-\tfrac{1}{2}\sigma_x(\tfrac{1}{3} - 2\alpha_x - \tfrac{1}{3}\sigma_x^2)\}\\
&+ c_{j,k-2,l}^{n}\{-\tfrac{1}{2}\sigma_y(\tfrac{1}{3} - 2\alpha_y - \tfrac{1}{3}\sigma_y^2)\}\\
&+ c_{j,k,l-2}^{n}\{-\tfrac{1}{2}\sigma_z(\tfrac{1}{3} - 2\alpha_z - \tfrac{1}{3}\sigma_z^2)\}\\
&+ c_{j-1,k-1,l}^{n}\{\sigma_x\sigma_y - \tfrac{1}{2}\sigma_y(-\sigma_x^2 - 2\alpha_x + \sigma_x) - \tfrac{1}{2}\sigma_x(-\sigma_y^2 - 2\alpha_y + \sigma_y) - \sigma_x\sigma_y\sigma_z\}\\
&+ c_{j-1,k,l-1}^{n}\{\sigma_x\sigma_z - \tfrac{1}{2}\sigma_z(-\sigma_x^2 - 2\alpha_x + \sigma_x) - \tfrac{1}{2}\sigma_x(-\sigma_z^2 - 2\alpha_z + \sigma_z) - \sigma_x\sigma_y\sigma_z\}\\
&+ c_{j,k-1,l-1}^{n}\{\sigma_y\sigma_z - \tfrac{1}{2}\sigma_z(-\sigma_y^2 - 2\alpha_y + \sigma_y) - \tfrac{1}{2}\sigma_y(-\sigma_z^2 - 2\alpha_z + \sigma_z) - \sigma_x\sigma_y\sigma_z\}\\
&+ c_{j+1,k-1,l}^{n}\{-\tfrac{1}{2}\sigma_y(-\sigma_x^2 - 2\alpha_x + \sigma_x)\}\\
&+ c_{j,k+1,l-1}^{n}\{-\tfrac{1}{2}\sigma_z(-\sigma_y^2 - 2\alpha_y + \sigma_y)\}\\
&+ c_{j+1,k,l-1}^{n}\{-\tfrac{1}{2}\sigma_z(-\sigma_x^2 - 2\alpha_x + \sigma_x)\}\\
&+ c_{j,k-1,l+1}^{n}\{-\tfrac{1}{2}\sigma_y(-\sigma_z^2 - 2\alpha_z + \sigma_z)\}\\
&+ c_{j-1,k,l+1}^{n}\{-\tfrac{1}{2}\sigma_x(-\sigma_z^2 - 2\alpha_z + \sigma_z)\}\\
&+ c_{j-1,k+1,l}^{n}\{-\tfrac{1}{2}\sigma_x(-\sigma_y^2 - 2\alpha_y + \sigma_y)\}\\
&+ c_{j-1,k-1,l-1}^{n}\{\sigma_x\sigma_y\sigma_z\} \qquad \text{(A3)}
\end{aligned}
$$

By recalling equations (3) and (4) and through inspection of equation (A3), the transport terms can be identified as

$$
\begin{aligned}
T_x(j,k,l) &= \delta_1 c_{j+1,k,l} + \delta_2 c_{j,k,l} + \delta_3 c_{j-1,k,l} + \delta_4 c_{j,k+1,l} + \delta_5 c_{j,k-1,l} + \delta_6 c_{j,k,l+1} + \delta_7 c_{j,k,l-1} + \delta_8 c_{j,k-1,l-1} \\
T_x(j-1,k,l) &= \delta_1 c_{j,k,l} + \delta_2 c_{j-1,k,l} + \delta_3 c_{j-2,k,l} + \delta_4 c_{j-1,k+1,l} + \delta_5 c_{j-1,k-1,l} + \delta_6 c_{j-1,k,l+1} \\
&\quad + \delta_7 c_{j-1,k,l-1} + \delta_8 c_{j-1,k-1,l-1} \\
T_y(j,k,l) &= \gamma_1 c_{j,k+1,l} + \gamma_2 c_{j,k,l} + \gamma_3 c_{j,k-1,l} + \gamma_4 c_{j+1,k,l} + \gamma_5 c_{j-1,k,l} + \gamma_6 c_{j,k,l+1} + \gamma_7 c_{j,k,l-1} + \gamma_8 c_{j-1,k,l-1} \\
T_y(j,k-1,l) &= \gamma_1 c_{j,k,l} + \gamma_2 c_{j,k-1,l} + \gamma_3 c_{j,k-2,l} + \gamma_4 c_{j+1,k-1,l} + \gamma_5 c_{j-1,k-1,l} + \gamma_6 c_{j,k-1,l+1} \\
&\quad + \gamma_7 c_{j,k-1,l-1} + \gamma_8 c_{j-1,k-1,l-1} \\
T_z(j,k,l) &= \beta_1 c_{j,k,l+1} + \beta_2 c_{j,k,l} + \beta_3 c_{j,k,l-1} + \beta_4 c_{j+1,k,l} + \beta_5 c_{j-1,k,l} + \beta_6 c_{j,k+1,l} + \beta_7 c_{j,k-1,l} + \beta_8 c_{j-1,k-1,l} \\
T_z(j,k,l-1) &= \beta_1 c_{j,k,l} + \beta_2 c_{j,k,l-1} + \beta_3 c_{j,k,l-2} + \beta_4 c_{j+1,k,l-1} + \beta_5 c_{j-1,k,l-1} + \beta_6 c_{j,k+1,l-1} + \beta_7 c_{j,k-1,l-1} \\
&\quad + \beta_8 c_{j-1,k-1,l-1}
\end{aligned}
\tag{A4}
$$

The weights can now be computed by using equation (A3) and symmetry conditions, that is, giving each direction a similar weight. The weights are listed in *Table 1*. The locations of the weights can be seen in *Figure 2*.

3 Dispersion Coefficients

3.1 General Description

Dispersion is commonly used as a general term to refer to the scattering of fluid particles that depend both on random-type processes (diffusion) and on the effect of velocity gradients (shear), as schematised in Table 3.1. The diffusive processes are never resolved, which led to early attempts by Fick (1855) and Taylor (1921) to parameterise the mass fluxes of solutes due to molecular and turbulent motions, respectively. They assumed that the mass fluxes could be set to be proportional to the concentration gradients, the constants of proportionality being called the molecular and turbulent diffusion coefficients, respectively. Taylor (1953, 1954) extended this approximation to shear flows, the combined effect of differential advection and diffusion being thus represented by the so-called dispersion coefficients. Elder (1959) applied Taylor's analysis to shallow water flows in order to describe the shear effects of the vertical velocity gradients.

The concept of dispersion of mass of any substance in solution or suspension in a flow can be extended to other properties of the flow. Resorting to Backmeteff's principle of momentum transfer, it follows that the velocity fluctuations act as a mechanism of transfer of momentum between adjacent scales of circulation, i.e. they provide for the dispersion of momentum. The corresponding coefficients are the so-called viscosity coefficients.

Table 3.1 Transport of Fluid Particles

<table>
<tr><th colspan="2">MAIN TRANSPORT PROCESSES</th></tr>
<tr><td colspan="2">ADVECTION
Movement of fluid particles due to the resolved flow processes</td></tr>
<tr><td rowspan="2">DISPERSION
Scattering of fluid particles due to non-resolved flow processes</td><td>SHEAR
Spatial velocity gradients</td></tr>
<tr><td>DIFFUSION
Molecular motion
Turbulence</td></tr>
</table>

3.2 Dispersive Processes

3.2.1 General

The commonly recognised filtering procedures used in the development of the momentum and transport-dispersion equations are:

Scale 1		
Filter out the random molecular motion	}	→ molecular diffusion → viscosity
Scale 2		
Filter out the turbulent motion below a given scale	}	→ turbulent diffusion → eddy-viscosity
Scale 3		
Depth averaging to filter out the vertical velocity profile for 2-D models	}	→ dispersion → bed & surface shear stresses → horizontal shear stresses - shear viscosity

Scale 1, which corresponds to filtering out the random molecular motions, is the basis of Newton's law of viscosity

$$\tau_{zx} = \mu \frac{\partial u}{\partial z} \tag{3.1}$$

where viscosity μ may be regarded as a measure of the resistance of the flow to deformation imposed by tangential stresses τ, which are generated by the transfer of momentum due to velocity fluctuations normal to the corresponding surface. With respect to the fluctuations due to molecular motions, their effect on the transfer of momentum is independent of the flow conditions, thus the dynamic viscosity μ is a characteristic of the fluid. The corresponding dynamic equilibrium equations are the well-known Navier-Stokes equations, where the influence of the non-resolved scales of random molecular motions are accounted for by the following empirical terms (in the x_i direction)

$$\nu \left[\frac{\partial^2 u_i}{\partial x^2} + \frac{\partial^2 u_i}{\partial y^2} + \frac{\partial^2 u_i}{\partial z^2} \right], i = 1,2,3 \tag{3.2}$$

$\nu = \mu/\rho$ being the Kinematic viscosity (L^2 / T).

The random molecular motions also induce the transfer of mass of any substance dissolved or in suspension in the fluid, which according to Fick's law is given by

$$T_i = D^m \frac{\partial c}{\partial x_i} \tag{3.3}$$

where *c* represents the concentration of the constituent and *Dm* the molecular diffusion coefficient. Applying a conservation principle to an arbitrary volume of control, an empirical term similar to (3.2) will appear

$$D^m \left[\frac{\partial^2 c}{\partial x^2} + \frac{\partial^2 c}{\partial y^2} + \frac{\partial^2 c}{\partial z^2} \right] \tag{3.4}$$

3.2.2 Turbulence

Although molecular agitation is always present even for fluids at rest, under flow conditions fluid particles experience additional random motions of much higher magnitude, so that their paths are very irregular and sinuous. It is apparent when observing recorded time series of instantaneous velocities u^I, that the flow is characterised by an unsteady fluctuating velocity u' superimposed on a temporal steady mean velocity u, such that

$$u^I(x,t) = u(x,t) + u'(x,t) \tag{3.5}$$

$$\overline{u^I(x,t)} = \frac{1}{\Delta T} \int_{t-\Delta T}^{t} u^I(x,t)dt = u(x,t) \tag{3.6}$$

$$\overline{u^I(x,t)} = \frac{1}{\Delta T} \int_{t-\Delta T}^{t} u'(x,t)dt = 0 \tag{3.7}$$

In these conditions it is possible to filter out the fluctuations under a selected time scale ΔT, by integrating the Navier-Stokes equations over ΔT. As a result, the following new terms will be obtained

$$\frac{\partial}{\partial x_j} \left[\rho \overline{u_i' u_j'} \right] \tag{3.8}$$

Similarly for the conservation of property *c*, the result is,

$$\frac{\partial}{\partial x_j} \left[\rho \overline{u_i' c'} \right] \tag{3.9}$$

In the classical theory of turbulence the terms $-\rho u_i' u_j'$, called Reynold's stresses, are empirically correlated to the resolved scales through a new coefficient ν^T, the "eddy viscosity", such that

$$-\rho \overline{u_i' u_j'} = \rho \nu^T \frac{\partial u_i}{\partial x_j} \tag{3.10}$$

which makes it possible to write the new terms in the following form

$$\frac{\partial}{\partial x}\left[\nu^T \frac{\partial u_i}{\partial x}\right] + \frac{\partial}{\partial y}\left[\nu^T \frac{\partial u_i}{\partial y}\right] + \frac{\partial}{\partial z}\left[\nu^T \frac{\partial u_i}{\partial z}\right] \tag{3.11}$$

It is apparent that ν^T is now dependent on the flow conditions. For the evaluation of ν^T several models have been developed, each corresponding to a particular kind of turbulence (e.g. isotropy). One of the formulations adopted by DHI is based on the so-called Smagorinsky model of isotropic turbulence (1963), given by

$$\nu^T = \rho\, \ell^2(x_i)(S_{ij} S_{ji})^{1/2} \tag{3.12}$$

where $\ell(x_i)$ is a characteristic mixing length and S_{ij} the second order strain tensor. It is obvious that considering ν^T constant, expression (3.11) reduces to the form of expression (3.2) established for molecular motion (Boussinesq approximation).

In general it is difficult to determine ν^T but as a reference, for uniform channel flow it is often assumed to take a value given approximately by

$$\nu^T \approx \frac{1}{10} h\, u* \tag{3.13}$$

where h is the water depth and u* the friction velocity.

Introducing the Reynold's analogy for turbulent flows, that expresses the principle that the transfer processes of dissolved or suspended matter are equivalent to the transfer processes of momentum, and consequently the turbulent diffusion coefficient D^T will be such that $D^T \cong \nu^T$, the new dispersive terms of the conversation equation becoming

$$\frac{\partial}{\partial x}\left[D^T \frac{\partial c}{\partial x}\right] + \frac{\partial}{\partial y}\left[D^T \frac{\partial c}{\partial y}\right] + \frac{\partial}{\partial z}\left[D^T \frac{\partial c}{\partial z}\right] \tag{3.14}$$

3.2.3 Shear flows

For many coastal engineering applications where the depth is much smaller than the horizontal dimensions of the domain under study, two-dimensional models are usually adequate to describe the main flow processes. Nevertheless the depth-integration will imply the filtering of the vertical velocity profiles, which are responsible for additional spreading in the direction of the flow. Flows with velocity gradients are often referred to as "shear flows", and the associated spreading mechanism discussed by Taylor (1954) is currently known as the "shear effect". Hence, to account for "shear flows" in a depth integrated model (i.e. 2D), additional empirical terms have to be included.

The filtering procedure can now be based on the following relationships:

$$u = (U + U') \tag{3.15}$$

$$\overline{U'} = \frac{1}{h}\int_h^\xi U' dz = 0 \tag{3.16}$$

$$\bar{u} = \frac{1}{h}\int_{\xi}^{h}(U + U')dz = U \tag{3.17}$$

where U represents the depth-integrated velocity and U' the deviation of the velocity profile from the average velocity U, at a general depth z.

Introducing these relationships in the Reynolds equations (Navier-Stokes equations after filtering out turbulence under a time scale ΔT), it is possible to demonstrate that the convective terms will be given by

$$\frac{\partial}{\partial x}\int_{-h}^{\zeta} uudz + \frac{\partial}{\partial y}\int_{-h}^{\zeta} vudz = \tag{3.18}$$

$$\frac{\partial}{\partial x}(hUU) + \frac{\partial}{\partial y}(hVU)\frac{\partial}{\partial x}\int_{-h}^{\zeta}(u')^2\,dz + \frac{\partial}{\partial y}\int_{-h}^{\zeta}(u'v')^2\,dz$$

The last two terms represent the overall transfer of momentum over the depth due to the shear effect, and in an assumption similar to that applied to the turbulent transfer of momentum, it is common to accept the following correlations with the resolved dependent variables (depth-integrated):

$$\frac{1}{h}\int_{-h}^{\zeta}(U')^2\,dz = -\nu_x^s\frac{\partial U}{\partial x} \tag{3.19}$$

and

$$\frac{1}{h}\int_{-h}^{\zeta}(U'V')\,dz = -\nu_y^s\frac{\partial U}{\partial y} \tag{3.20}$$

The above assumptions and the Reynolds analogy make it possible to finally write the new terms for the conservation of momentum and constituents in the following form

$$\frac{\partial}{\partial x}\left[\nu_i^s h\frac{\partial U_i}{\partial x}\right] + \frac{\partial}{\partial y}\left[\nu_i^s h\frac{\partial U_i}{\partial y}\right] + \frac{\partial}{\partial z}\left[\nu_i^s h\frac{\partial U_i}{\partial z}\right] \tag{3.21}$$

and

$$\frac{\partial}{\partial x}\left[D_i^s h\frac{\partial U_i}{\partial x}\right] + \frac{\partial}{\partial y}\left[D_i^s h\frac{\partial U_i}{\partial y}\right] + \frac{\partial}{\partial z}\left[D_i^s h\frac{\partial U_i}{\partial z}\right] \tag{3.22}$$

where $\nu_i^s \cong D_i^s$, with ν_i^s and D_i^s representing the horizontal shear stresses and dispersion in depth-integrated shear flows (in the x_i direction). The coefficient ν_i^s will be called hereafter the “shear viscosity”.

In the case of uniform channel flow (Abbott et al., 1976) the shear viscosity can be estimated by

$$v_i^s = D_i^s = \frac{\alpha - (\alpha')^2}{2} C_z U h \tag{3.23}$$

with

$$\alpha = \frac{\int_{-h}^{\zeta} u^3 dz}{U^3 h} \tag{3.24}$$

and

$$\alpha' = \frac{\int_{-h}^{\zeta} u^2 dz}{U^2 h} \tag{3.25}$$

where C_z is the non-dimensional Chézy number, U the depth-averaged velocity and h the water depth.

For example, considering a 10 meter deep channel with a depth- averaged velocity of 1 m/s and a non-dimensional Chézy number of 18, the shear viscosity coefficient that corresponds to an exponential velocity distribution along the vertical given by $KZ^{0.2}$ is ν^S = 4 m^2/s.

As expected, these results suggest that the intensity of transfer of momentum and constituents is related to the magnitude of the scale considered, the molecular and turbulent effects being in practice negligible in comparison to the shear effect (10^{-6} to 10^{-1} m^2/s against 4 m^2/s).

3.2.4 Subgrid scale processes

At this point it is convenient to emphasise that the concepts of viscosity and diffusion have been brought about by the need to take into account non-resolved motions of the fluid particles, i.e. diffusion and dispersion are the result of advective processes associated with non-resolved scales. This concept is the one that really matters when the filtering procedures are further extended to higher scales, as a consequence of the need for horizontal and vertical spatial discretisation of the equations. It implies that additional dispersion and viscosity will be required to account for higher order non-resolved scales of motion, which magnitude will be dependent on the grid spacing used in the numerical computations. Once again it is only natural to expect that by increasing the grid spacing, the dispersive coefficients will also increase, with practice confirming that they can be several orders of magnitude higher than e.g. the coefficients arising from depth-integration. In the case of depth-integration where the grid spacing is similar to water depth, $\Delta x \cong h$, the larger non-resolved scales of circulation will be related to the shear flow and the extensive studies available on this subject provide very accurate first estimates for the empirical coefficients, so long as the velocity profile is well defined, as will be shown in Section 3.3.1.

One of the main difficulties found when estimating dispersion coefficients, so as to take into account the horizontal spatial discretisations, is the characterisation of the new non-resolved scales of motion, which can be greatly dependent on factors like local bathymetric configurations, density gradients and wind friction and set-up. Although some

general formulae can be used for guidance, the accuracy of the final values will always be greatly dependent on calibration and on the experience of the modeller.

In conclusion, the fact that the numerical resolution of the primitive equations has to resort to additional discretisations in space and time (generally, no analytical solutions are available), makes it necessary to extend filtering to larger scales of motion which are dependent on the model resolution, Δx and Δz. Thus, following the previous schematisation a fourth scale must be considered, such that

Scale 4

Averaging over the model resolution Δx, Δt } → additional dispersion
→ additional viscosity

In what follows the additional dispersion and viscosity will be referred to as Subgrid Dispersion D^G and Subgrid Viscosity ν^G.

3.3 Estimation of Coefficients in 2D Modelling

3.3.1 Basic formulations

The general advection-dispersion equation reads

$$\frac{\partial c}{\partial t}+\frac{\partial u_i c}{\partial x_i}=\frac{\partial}{\partial t}\left(D_i\frac{\partial c}{\partial x_i}\right)+SS \tag{3.26}$$

Where c is the concentration, D_i the dispersion coefficient and SS a possible source term.

As a basis for the interpretation of dispersive coefficients in 2D, Elder's formulation will be used. Consider the mass conservation equation for a dissolved constituent in an open channel of infinite lateral extent, where the lateral and vertical velocity components are zero and the horizontal diffusion can be neglected. Equation (3.27) can then be written

$$\frac{\partial c}{\partial t}+\frac{\partial}{\partial x}(uc)=\frac{\partial}{\partial z}\left[\,D_z^T\frac{\partial c}{\partial z}\,\right] \tag{3.27}$$

Considering the vertical profile defined by equations (3.15) - (3.17) and taking into account the flux continuity for incompressible fluids, equation (3.27) can be written

$$\frac{\partial}{\partial t}(C+C')+(U+U')\frac{\partial}{\partial x}(C+C')=\frac{\partial}{\partial z}\left[\,D_z^T\frac{\partial C'}{\partial z}\,\right] \tag{3.28}$$

Introducing now a non-inertial frame of reference moving at velocity U, C and C' will be functions of $x' = x - Ut$ and $t' = t$, which brings the previous equation to the following form

$$\frac{\partial}{\partial t}(C+C')+U'\frac{\partial}{\partial x'}(C+C')=\frac{\partial}{\partial z}\left[\,D_z^T\frac{\partial C'}{\partial z}\,\right] \tag{3.29}$$

After a sufficiently long time, *C* and *C'* will become functions only of *x'* and *t*, respectively, which make it possible to finally write

$$U' \frac{\partial C}{\partial x'} = \frac{\partial}{\partial z}\left[D_z^T \frac{\partial C'}{\partial z} \right], t \to \infty \tag{3.30}$$

Proceeding by integrating the previous equation, one gets

$$C' = \left[\int_0^z \frac{1}{D_z^T} \left(\int_0^z U' \, dz \right) dz \right] \frac{\partial C}{\partial x'} \tag{3.31}$$

Multiplying by *U'* and integrating again over the vertical, it yields

$$\frac{1}{h} \int_0^h (U'C') \, dz = \frac{\partial C}{\partial x'} \frac{1}{h} \left\{ \int_0^h U' \left[\int_0^z \frac{1}{D_z^T} \left(\int_0^z U' dz \right) dz \right] dz \right\} \tag{3.32}$$

and it is now clear that the dispersion coefficient can be given by

$$D_x^s = \frac{1}{h} \left\{ \int_0^h U' \left[\int_0^z \frac{1}{D_z^T} \left(\int_0^z U' dz \right) dz \right] dz \right\} \tag{3.33}$$

Elder evaluated D_x^s using Von Karman's logarithmic profile for the velocity

$$U'(z) = \frac{u^*}{\kappa} \left[1 + ln \frac{z}{h} \right] \tag{3.34}$$

where u^* is the shear velocity $(\tau_o / \rho)^{1/2}$ and κ(~ 0.41) the Von-Karman constant. The shear stress distribution is considered to be linear

$$\tau = \tau_o \, (1 - z/h) \tag{3.35}$$

and the assumption is made that the turbulent transport of mass and momentum are identical (Reynold's analogy). Noting also that the vertical turbulent momentum transfer is given by

$$\tau = \rho \, \nu_z^T \frac{\partial U'}{\partial z} \tag{3.36}$$

it transpires that

$$D_z^T = \nu_z^T = u^* \kappa \, z \, (1 - \frac{z}{h}) \tag{3.37}$$

Considering now the independent variable in equation (3.33) given by $\zeta = z/h$ and taking into account (3.34) and (3.37), Elder obtained

$$D_x^s = \frac{u^* h}{\kappa^3} \left\{ \int_0 (1+ln\zeta) \left[\int_0^{\zeta} \frac{(1+ln\zeta)d\zeta}{\zeta(1-\zeta)} d\zeta \right] d\zeta \right\} \quad (3.38)$$

Performing the integration, one gets

$$D_x^s = 0.404 \frac{u^* h}{\kappa^3} = K_E u^* h \quad (3.39)$$

with K_E = 5.9 and κ = 0.41.

Expressions similar to Elder's have been proposed with a wide variety of coefficients, as for example

Krenkel (1962) for open channel flow:	9.1 $u^* h$
Yotsukura & Fiering (1964) for smooth channels:	13 $u^* h$
Thackston (1966) for natural streams:	7.25 $(u/u^*)^{1/4}$ $u^* h$

to mention but a few, as presented by Bansal (1971).

Jobson and Sayre (1970) have provided some evidence that the Reynolds analogy holds (i.e. $\nu^T/D^T \cong 1$). They also confirmed the parabolic distribution of ν^T and found that the mean depth value was about

$$D_z^T = 0.07 \; u^* h \quad (3.40)$$

which justifies its being neglected in comparison to horizontal dispersion due to shear flows.

In applications for natural streams, Fischer (1968) found that longitudinal dispersion coefficients as predicted by Elder's formula were too small, values as much as 150 times higher having been reported. Bowden (1964) pointed out that the effective coefficients of horizontal dispersion are inversely proportional to the coefficient of vertical turbulent diffusion, which is also apparent in Elder's development (3.33). The mixing produced under a shearing current will thus be enhanced if some stability factors are present in the vertical, their effects becoming important for local Richardson numbers of about 0.5 to 1. According to Bowden the coefficient of vertical turbulent diffusion may then be reduced by a factor of 10 or 20, with a corresponding increase in the horizontal dispersion coefficients, to an order of 10^5 to 10^6 cm²/sec.

The conclusions of these authors clearly show that other mechanisms of spreading may be dominant in comparison with shear effects. Fischer proposed that the main factor contributing to longitudinal dispersion was transversal diffusion and not vertical diffusion, i.e. the dominant mechanism of spreading should be associated with transversal circulations (this analysis having been done for natural streams). Bowden recognised that shear effects are likely to be most effective in estuaries and near the coastline, and that the existence of large horizontal eddies may dominate among the dispersion processes.

3.3.2 The evidence of experience

It is well demonstrated that dispersive effects due to physical processes at scales 1 and 2 are negligible in relation to those at scale 3. With respect to environmental flows, field measurements and modelling results also show that in most situations Elder's coefficient is several orders of magnitude too small as mentioned previously. This is illustrated in Table 3.2, in which calibrated coefficients are compared with Elder's formula for 4 different applications with a two-dimensional circulation model (MIKE 21)

Table 3.2 Comparison between Elder's coefficient and calibrated coefficient

Case	*h* m	*u* m/s	*u** m/s	Δ*x* m	Δ*t* s	E. calib. m^2s	6.*hu** m^2/s
A	8	0.7	0.05	50	30	2-5	2.4
B	20	1.0	0.1	500	300	40-50	12
C	30	0.5	0.03	6000	600	~500	5.4
D	1000	0.1	0.003	30000	900	>6000	18

The magnitude of the calibrated coefficients can only be explained by considering processes at Scale 4, that for values of $\Delta x >> h$ usually dominate over processes in Scale 3.

Many modellers attempt to account for the filtered processes at Scale 4 by increasing the coefficient K_E in Elder's formulation, which will only be acceptable as long as those processes remain related to flow variations in the vertical. However, to represent subgrid processes it is only natural to relate the effective coefficients of viscosity and dispersion to the length scale Δx and to the time scale Δt. Hence the effective coefficients for subgrid processes may be considered in the following possible forms:

$$K_1 \quad \frac{\Delta x^2}{\Delta t} \tag{3.41}$$

$$K_2 \quad \Delta x \quad u \tag{3.42}$$

$$K_3 \quad \Delta t \quad u^2 \tag{3.43}$$

In Table 3.3 the three different forms of the effective coefficient for Scale 4 have been compared to calibrated results in five different situations.

Table 3.3 Effective coefficients of scale 4

CASE	h (m)	u (m/s)	Δx (m)	Δt (s)	$E_{cal.}$ (m2/s)	K_1	K_2	K_3
A	8	0.7	50	30	1-5	0.06-0.01	0.14-0.03	0.34-0.07
B	20	1.0	500	300	40-50	0.06	0.10	0.17
C	30	0.5	6000	600	~500	0.008	0.17	3.3
D	40	1.0	20	10	1-3	0.075-0.025	0.15-0.05	0.30-0.10
E	1000	0.1	30000	900	~6000	0.006	2.0	667

The form $K_2 \Delta x\, u$ appears to be promising since K_2 is almost constant in the five different cases.

It is important to emphasise that as equations (3.41) - (3.43) are not based on a defined pattern of circulation, like Euler's formulation, the estimates can only be expected to be a rough approximation to the true values. Furthermore, as will be analysed in the next section, the values of the dispersive coefficients are dependent on the biggest non-resolved circulations, and not directly on Δx or Δt. This is very important, and makes it possible to justify that in situations where $\Delta x >> h$, the use of Elder's formulation may still be valid although the associated dispersive processes will be irrelevant in comparison with other effects. Nevertheless, the above formulae, when complemented with field observations and experience obtained in similar situations, do provide valuable guidance for the calibration of two-dimensional environmental models.

When Δx and h are of the same order of magnitude, the shear effects (processes at Scale 3) will be the ones responsible for the transfer of momentum and constituents. In practice, assuming that the friction velocity for coastal waters is about 6% of the mean depth velocity, Elder's formula will give

$$\nu_x^s \cong D_x^s \cong 5.9 \cdot 0.06\, U\, h \cong 0.4\, U\, h \tag{3.44}$$

Thus, for application in MIKE 21 when $\Delta x \cong h$ the dispersive coefficients (shear viscosity and dispersion) are taken as a first approximation as, to be

$$\nu_x^s \cong D_x^s \cong 1.0\, U\, h \tag{3.45}$$

with the factor 1.0 possibly varying by one order of magnitude according to calibration.

It should be stressed that in the above discussion direction x was assumed to be aligned with the flow direction, the coefficients thus obtained being representative of the longitudinal dispersive processes. In the case of shear effects the transverse or lateral processes are found to be approximately one order of magnitude smaller than the longitudinal ones, as indicated by tests reported by Talbot & Talbot (1974). For an arbitrary direction of the flow in a Cartesian coordinate system, cross terms would then be present, complicating the definition of the coefficients. Calling D_L^s, D_T^s longitudinal and lateral coefficients, a reasonable approach would be to project them on the x and y directions and disregard cross derivative terms. This can be accomplished by taking the

ellipse of semi-axes D_L^s, D_T^s in which D_L^s is aligned with the current vector (*u,v*), and calculate D_x^s and D_y^s accordingly, eventually obtaining

$$\frac{1}{D_x^s} = \left[\left(\frac{\cos\alpha}{D_L^s} \right)^2 + \left(\frac{\sin\alpha}{D_T^s} \right)^2 \right]^{1/2} \tag{3.46}$$

$$\frac{1}{D_y^s} = \left[\left(\frac{\sin\alpha}{D_L^s} \right)^2 + \left(\frac{\cos\alpha}{D_T^s} \right)^2 \right]^{1/2} \tag{3.47}$$

Where

$$\alpha = \arctan(v/u) \tag{3.48}$$

However, for dispersive processes associated with the largest scales, as is the case in subgrid flow circulations, the influence of flow direction is no longer relevant, which means that isotropy can be usually assumed.

3.3.3 A general interpretation

Abbott et al. (1985) showed that it is possible to simulate realistically secondary large scale circulations by using two-dimensional models. Madsen et al. (1988) continuing on the same subject referred to the existence of two fundamental mechanisms for the generation of circulations, where the resistance forces (bottom friction) are balanced by:

- the momentum transfer resolved at the scale of the spatial discretisation adopted (convective accelerations)
- the momentum transfer non-resolved at the scale of the spatial discretisation adopted, represented by horizontal shear stresses ("subgrid viscosity")

The first mechanism is dominant in many situations where the scales of flow circulation and space discretisation Δx are much bigger than the depth of the flow, and the second one is fundamental to describe secondary circulations when $\Delta x \leq h$. Nevertheless, for some situations where $\Delta x >> h$ it is found in practice that the second mechanism is still necessary to describe the resolved scales of circulation. A possible explanation may be found in the following heuristic hypothesis:

- The transfer of momentum or constituents amongst resolved scales depends upon the relative magnitude of the minimum resolved scale and the maximum non-resolved scale. The transfer is only effective when these scales have the same order of magnitude.

To analyse the consistency of this statement the following interpretations are made:

1. When the structure of the flow is well defined by a logarithmic profile of velocities and Δx is of the same order of magnitude of the depth h, the biggest non-resolved scale is the velocity profile itself, Elder's formula being thus valid for the estimation of the effective viscosity and dispersion coefficients. The second mechanism is fundamental to describe flow circulation.

2. When $\Delta x >> h$ several situations may be found:

   a. The bottom is very regular and three-dimensional effects are negligible. In this case the biggest non-resolved scale will still be related to the depth, thus being much smaller than the minimum resolved scale. Consequently the transfer of momentum due to the non-resolved scales (subgrid viscosity) is negligible. Euler's formula is still valid but the model will not be sensitive to the values of the viscosity coefficient. The circulation is only determined by the first mechanism, i.e., by the dissipative terms, as the non-resolved scales only contribute as energy absorbers.

   b. The bottom configurations and the existence of three-dimensional effects originate circulations, the scales of which are of the same order of magnitude of Δx, i.e., important in relation to the minimum resolved scales. In this case the transfer of momentum due to the non-resolved scales becomes significant. This can be easily illustrated by the experience of many authors, who for calibration of regional models using large grid spacings ($\geq$ 5000 m) employed dispersion coefficients proportional to Δx or/and h. As an example one of the formulae commonly used is given by $E = K\,\Delta x^2/\Delta t$ with $0.01 < K < 0.06$. For a regular mesh with a 30,000 m grid spacing, a 15 min. time step and an average depth of 1000 m, we get $10{,}000 < E < 60{,}000$ m²/s, i.e. 10 h $< E <$ 60 h.

      Schwiderski (1978), for his global oceanic tidal model used a dispersion coefficient linearly proportional to the depth and -x, which gives values consistent with the previous formula.

3. It is logical to expect that by using the Prandtl model for the determination of the dispersive coefficients, the mixing length will be related to the magnitude of the maximum non-resolved scales. Using the Smagorinsky formulation and considering the mixing length given by

$$\ell = C_s \Delta x \tag{3.49}$$

Madsen et al. (1988) recommended values of C_s in the range (0.4 - 0.8). These values are consistent with the hypothesis formulated before, i.e., the transfer processes of momentum and constituents are only important when the non-resolved circulations are of the same order of magnitude as Δx.

4 Heat Dissipation

In the heat balance for a free surface the following items are included: net short-wave radiation (from the sun), net long-wave radiation (e.g. from clouds), long-wave outgoing radiation from the surface (Stefan-Bolzmanns law), evaporation and heat exchange to the air as a function of the temperature difference between water and air (convection).

In connection with an artificially warmed aquatic area, the loss of heat will increase due to long-wave radiation, evaporation and convection. This increase in heat loss is included as a decay term in the calculation of the excess temperature field, $F \cdot T$, where F is the heat decay coefficient and T the excess temperature. The following simplified expression is used for calculating the decay coefficient

if $W \geq W_{min}$:

$$F = 0.2388/\left(\rho \cdot C_p \cdot H\right)\left(4.6 - 0.09\left(T_r + T\right) + 4.06 \cdot W\right) \exp\left(0.033\left(T_r + T\right)\right) + 0.2388K_{shift}/\left(\rho \cdot C_p \cdot H\right) \quad (4.1)$$

if $W<W_{min}$:

$$F = 0.2388/\left(\rho \cdot C_p \cdot H\right)\left(\left(\left(4.6 - 0.09\left(T_r + T\right) + 0.06 \cdot W_{\min}\right) \exp\left(0.03\left(T_r + T\right)\right) - K_{\min}\right)\left(\frac{W_{\min}}{W}\right)^2 + K_{\min} + K_{shift} \right) \quad (4.2)$$

where

Ψ	density of water
C_p	specific heat
H	water depth [m]
T_r	reference temperature [°C]
T	excess temperature [°C]
W	wind speed [m/s]

$\Psi \cdot C_p$ gives the value 10^6 Cal/m^3 °C in the program.

W_{min}, K_{min} and K_{shift} are by default 0.0, but can be specified by an option file.

The above expression is not valid for water surfaces with high excess temperatures, e.g. cooling water reservoirs.

5 Flooding and Drying

If the AD module is applied together with flooding and drying, then concentrations must be calculated every time a cell is flooded, and the mass of the AD compounds stored every time a drying sets in.

The HD modelling concepts at flooding/drying are described in MIKE 21 HD Scientific Background. The related AD modelling concepts at flooding/drying are described in the following sections.

5.1 General

When performing an AD calculation while using the flooding and drying functionality it is necessary to book-keep the mass of the AD component (or MIKE ECO Lab State Variable or MT fraction) in order to obtain an AD mass balance – similar in concept to the handling of water depths in the HD simulation in order to obtain a water volume/mass balance.

The AD functionality utilises 2 arrays at runtime:

- ***c(j,k)*** (data structure used to bookkeep of concentrations while cells are wet/flooded)
- ***ad_mass(j,k)*** (data structure used to bookkeep AD mass per area while cells are dry)

While a cell is wet *c(j,k)* will be directly updated by the AD equations of motion.

While a cell is dry *ad_mass(j,k)* will be updated with respect to mass per area when sources, models, rain with concentrations are added to cell *(j,k)* while it is dry. When HD mass violations takes place out of known reasons (water depth below EPSF) then ad_mass(j,k) will be updated accordingly and be subject to a corresponding mass per area violation.

We store the latest known AD mass per area in cell *(j,k).* The mass per area is what should be conservative during the simulation – normally we understand that the mass should be conserved, but since the area of the MIKE 21 computational cells have a uniform area equal to *dx*dy*, we might as well say that mass per area is what should be conservative.

5.2 Flooding due to External Sources

Flooding of a grid cell may be due to accumulation of water from external sources (Rain, Sources, External model contributions). In this case, if it takes N water increments (generally the same as number of taken time steps) to flood an initially dry cell *(j,k)*, then the concentration of the AD component in cell *(j,k)* at the time of the flooding will be modelled according to a weighted average:

$$c(j,k) = \frac{\sum_{n=1}^{N} c_n \cdot \Delta h_n}{\sum_{n=1}^{N} \Delta h_n} \quad (5.1)$$

Where Δh_n is the water increment and c_n is the concentration in the external source.

The initial imaginary water with water depth EPSF in this concentration modelling is ignored as we only take into account the concentration from the actual external contributions: the fallen precipitation, the added water from sources or from coupled models.

5.3 Flooding due to a High Water Level in Neighbour Cells

Flooding of a grid cell can also be due to a high water level in neighbour cells (water chain expansion/chain flooding). In this case the calculation of the concentration depends on the previous simulation steps.

5.3.1 Chain flooding for the first time

If a cell *(j,k-1)* – call it cell 1 - leads to a chain flooding of its neighbour cell *(j,k)* then the concentration at cell *(j,k)* will be calculated as the average of the neighbour concentrations in the neighbour wet cells. The general formula is highlighted below in Figure 5.1. If all 4 neighbour cells are dry when the concentration in *(j,k)* is about to be set, then we set *c(j,k) = c(j,k-1)* – e.g. we set the concentration in (j,k) to the original concentration value in cell *(j,k-1)* – the cell that triggered that cell *(j,k)* got flooded.

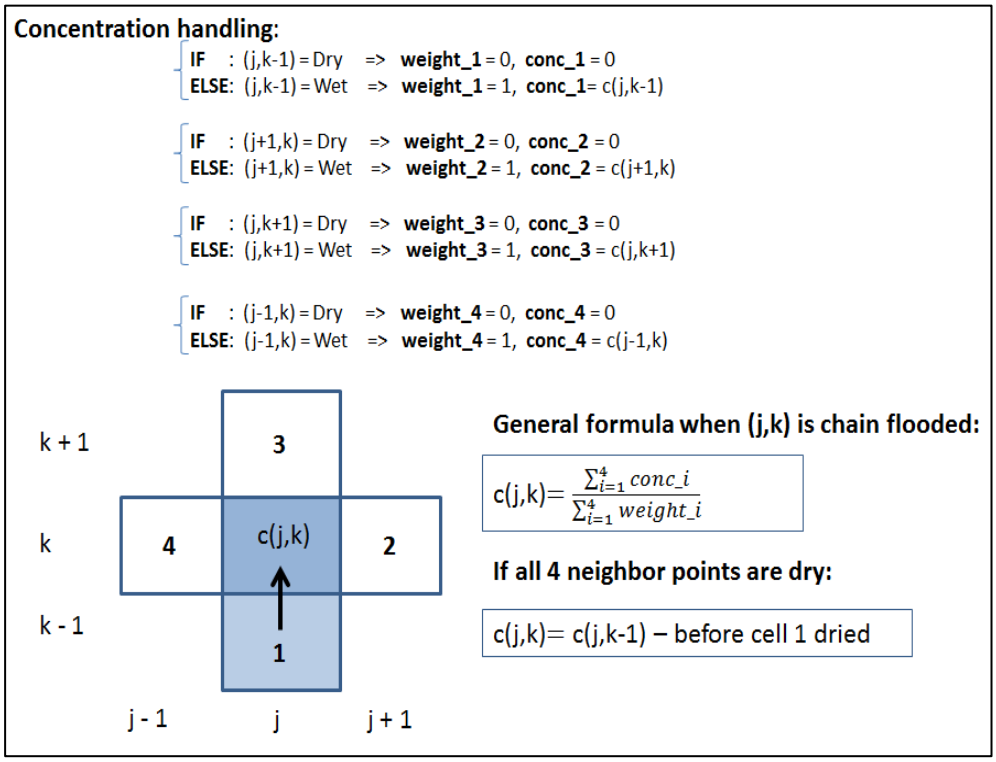

Figure 5.1 Illustration of concentration handling in case of first-time chain flooding

5.3.2 Chain flooding on previously wet cell

If a cell that was previously wet and later became dry is chain flooded again, the latest updated values for *ad_mass(j,k)* and *h_flood_dry(j,k)* are used to derive the concentration at flooding time:

$$c(j,k) = \frac{ad\_mass(j,k)}{h\_flood\_dry(j,k)} \tag{5.2}$$

5.4 Drying

When drying of a cell *(j,k)* sets in, and then the mass per area of the AD component (or MIKE ECO Lab State Variable or MT fraction) is stored as follows:

$$ad\_mass(j,k) = c(j,k) \cdot h\_flood\_dry(j,k) \tag{5.3}$$

6 List of Symbols

τ	Shear stresses
ρ	Density
μ	Dynamic Molecular Viscosity
ν	Kinematic Molecular Viscosity
ν^T	Kinematic Turbulent Viscosity
ν^S	Kinematic Shear Viscosity
D^m	Molecular Diffusion
D^T	Turbulent Diffusion
D^S	Shear Diffusion - Dispersion
K_E	Euler's coefficient
κ	Von Karman's constant
u^I	Instantaneous Velocity
u	Time-integrated Velocity
u'	Velocity Fluctuation
u^*	Shear Velocity
U	Depth-integrated Velocity
U'	Depth-integrated Velocity Fluctuation
c	Time-integrated Concentration
c'	Fluctuation of Concentration
C	Depth-integrated Concentration
C'	Depth-integrated Fluctuation of Concentration
ℓ	Mixing Length
S	Angular Deformation Tensor
h	Flow Depth
ζ	Water Surface Position
z	Vertical Direction

7 List of References

/1/ Abbott, M.B. et al. (1985): *Modelling circulations in Depth-integrated flows. Part 1: The accumulation of the evidence* J. Hyd. Res., Vol. 23, No. 4.

/2/ Bansal, M.K. (1971): *Dispersion in natural streams*. J. Hyd. Div., Proc. ASCE. HY11, pp. 1867-1886.

/3/ Bowden, K.F. (1965): *Horizontal Mixing in the sea due to a shearing current*. J. Fluid Mech, Vol 21, Part 2, pp. 83-95.

/4/ Elder, J.W. (1959): *The dispersion of a marked fluid in a turbulent shear flow*. J. Fluid Mech., 5, pp. 544-560.

/5/ Fischer, H.B. et al. (1979): *Mixing in Inland and Coastal Waters*. Academic Press.

/6/ Jobson, H.E. and Sayre, W.W. (1970): J. Hyd. Div., Proc. ASCE, Vol. 96, pp. 703-724.

/7/ Justesen, P. (1990): *System 3. A three-dimensional hydrodynamic model. Turbulence modelling*. Vol. 5. Danish Hydraulic Institute.

/8/ Leslie, D.C (1982): *Simulation methods for turbulent flows*. In Numerical Methods for Fluid Dynamics. Ed: Morton, K.W. and Baines, H.J., Academic Press, pp 63-80.

/9/ Leonard, A. (1974): *Energy cascade in large-eddy simulations of turbulent fluid flows*. Adv. in Geophysics, A, 18, pp. 237-248.

/10/ Madsen, P.A. et al. (1988): *Subgrid modelling in depth integrated flows* 21st. Int. Conf. on Coastal Engineering, Malaga.

/11/ Schumann, V. (1975): *Subgrid scale model for finite difference simulations of turbulent flows in plane channels and annuli*. J. Comput. Phys., Vol. 18, pp. 376-404.

/12/ Schwiderski, E.W. (1981): *Global Ocean Tides*. NSWC TR81-122. Chief of Naval Material, Department of the Navy, Washington, DC 20360.

/13/ Smagorinsky, J. (1963): *General Circulation experiments with the primitive equations, 1, The basic experiment*. Mon. Weather Rev., Vol. 91, pp. 90-164.

/14/ Thackson, E.L. (1966): *Longitudinal Mixing and Re-aeration in natural streams*. PhD Thesis, Vanderbilt University, Nashville, Tenesse.

/15/ Talbot, J.W. and Talbot, G.A. (1974): *Diffusion in shallow seas in English coastal and estuarine waters*. In Physical Processes Responsible for Dispersal of Pollutants in the Sea. Ed. G. Kullenberg and Talbot, J.W. International Council for Sea Exploration, pp. 93-110.

/16/ Taylor, G.I. (1954): *The dispersion of matter in turbulent flow through a pipe*. Proc. Royal Soc. London, Serv. 223-A, pp. 446-468.

/17/ Vieira, J.R. (1992): *On the general dispersive coefficients used in mathematical models of flow circulation and transport*. Coastal, Estuarial and Harbour Engineer's Reference Book. In press.